Accepted Manuscript

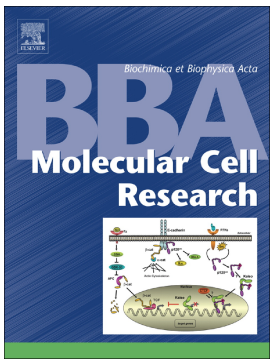

Novel short isoforms of adenylyl cyclase as negative regulators of cAMP production

Benjamin Vallin, Yohan Legueux-Cajgfinger, Nathalie Clément, Martine Glorian, Laurent Duca, Pierre Vincent, Isabelle Limon, Régis Blaise

PII: S0167-4889(18)30140-X
DOI: doi:10.1016/j.bbamcr.2018.06.012
Reference: BBAMCR 18304

To appear in: *BBA - Molecular Cell Research*

Received date: 29 January 2018
Revised date: 15 June 2018
Accepted date: 20 June 2018

Please cite this article as: Benjamin Vallin, Yohan Legueux-Cajgfinger, Nathalie Clément, Martine Glorian, Laurent Duca, Pierre Vincent, Isabelle Limon, Régis Blaise , Novel short isoforms of adenylyl cyclase as negative regulators of cAMP production. Bbamcr (2018), doi:10.1016/j.bbamcr.2018.06.012

This is a PDF file of an unedited manuscript that has been accepted for publication. As a service to our customers we are providing this early version of the manuscript. The manuscript will undergo copyediting, typesetting, and review of the resulting proof before it is published in its final form. Please note that during the production process errors may be discovered which could affect the content, and all legal disclaimers that apply to the journal pertain.

ACCEPTED MANUSCRIPT

Novel short isoforms of adenylyl cyclase as negative regulators of cAMP production

Authors:

Benjamin Vallin[1], Yohan Legueux-Cajgfinger[1], Nathalie Clément[1], Martine Glorian[1], Laurent Duca[2], Pierre Vincent[1,†,*], Isabelle Limon[1,†,*] and Régis Blaise[1,†].

1: Sorbonne Université, Université Pierre et Marie Curie (UPMC), Institut de Biologie Paris-Seine (IBPS), UMR CNRS 8256 Adaptation biologique et vieillissement (B2A), 75005 Paris, France.

2: UFR Sciences Exactes et Naturelles, Université de Reims Champagne Ardenne (URCA), UMR CNRS 7369 Matrice Extracellulaire et Dynamique Cellulaire (MEDyC), Laboratoire Signalisation et Récepteurs Matriciels (SiRMa), Campus Moulin de la Housse, 51687 Reims, France.

†: P.V, I.L and R.B equally contributed to this work.

*: to whom correspondence should be addressed: pierre.vincent@upmc.fr, isabelle.limon@upmc.fr

Phone: +33 (0)1 44 27 37 16 / 25 88

Fax: +33 (0)1 44 27 26 50

Running title: Short adenylyl cyclases downregulate cAMP

ACCEPTED MANUSCRIPT

ACCEPTED MANUSCRIPT

Abstract

Here, we cloned a new family of four adenylyl cyclase (AC) splice variants from interleukin-1β (IL-1β)-transdifferentiated vascular smooth muscle cells (VSMCs) encoding short forms of AC8 that we have named "AC8E-H". Using biosensor imaging and biochemical approaches, we showed that AC8E-H isoforms have no cyclase activity and act as dominant-negative regulators by forming heterodimers with other full-length ACs, impeding the traffic of functional units towards the plasma membrane. The existence of these dominant-negative isoforms may account for an additional unsuspected degree of cAMP signaling regulation. It also reconciles the induction of an AC in transdifferentiated VSMCs with the vasoprotective influence of cAMP. The generation of alternative splice variants of ACs may constitute a generalized strategy of adaptation to the cell's environment whose scope had so far been ignored in physiological and/or pathological contexts.

Keywords: short adenylyl cyclases / cAMP signaling / dominant-negative / heterodimerization / vascular smooth muscle cells.

ACCEPTED MANUSCRIPT

ACCEPTED MANUSCRIPT

1. Introduction

Cells responses to the environment depend on the expression and membrane localization of adenylyl cyclases (ACs), which, together with cyclic nucleotide phosphodiesterases (PDEs) and multidrug resistance-associated proteins (MRPs), are the principal enzymes controlling the cAMP signal. Nine membrane forms of ACs have been identified in mammals, with discrete tissue distributions and unique regulatory properties, providing a potential focal point within the cell for the integration of diverse stimuli [1,2]. It has been shown that changes in the AC population expressed in hamster *vas deferens* smooth muscle cells modify the processing of stimulatory and inhibitory inputs from α_2-adrenoceptors [3]. In vascular smooth muscle cells (VSMCs), *i)* the effect of vasopressin on cAMP production induced by β-adrenoceptor activation depends on the nature of the Ca^{2+}-sensitive AC isoforms expressed [4], *ii)* AC6 but not AC1, 2 or 5 overexpression induces cAMP-dependent cytoskeletal reorganization [5], *iii)* AC6 promotes hyaluronan-mediated intimal thickening of the *ductus arteriosus*, whereas AC2 inhibits AC6-induced hyaluronan production [6].

We have shown *in vitro* that the transdifferentiation of rat VSMCs towards a migratory/inflammatory phenotype in response to the pro-atherogenic cytokine interleukin-1β (IL-1β) is dependent on the *de novo* expression of AC8 [7,8]. By contrast, in a non-inflammatory context, differentiated/contractile VSMCs mostly express AC isoforms 3, 5, and 6 [4,9]. In the rat carotid artery balloon injury model, we have demonstrated that post-angioplasty restenosis is associated with a marked transient upregulation of AC8 expression in VSMCs migrating to form the intimal cushion [10]. In a mouse model of atherosclerosis, knocking out the AC8 gene decreases the inflammation of the abdominal aorta (Limon unpublished) and atherosclerotic lesions [11]. We have expanded these *in vivo* findings by showing, on human samples, that neointimal VSMCs display high levels of AC8, whereas very few AC8-positive VSMCs are detected in the medial layer in either atherosclerotic or healthy arteries [10].

This increase in AC expression in transdifferentiated VSMCs (tdVSMCs) initially appeared counterintuitive. Indeed, increases in intracellular cAMP concentration ($[cAMP]_i$) have been shown to inhibit the migratory, proliferative and inflammatory properties of tdVSMCs [12–19]. In addition, several *in vivo* studies have shown that increases in $[cAMP]_i$ in tdVSMCs antagonize pathological vascular remodeling [20–23].

ACCEPTED MANUSCRIPT

Four different splice variants of AC8, encoding the AC8A-D isoforms, have been identified in human, mice and/or rat so far [24–27]. AC8A-D all display different structure, subcellular location and enzymatic activity [24,26]. We show here that the AC expressed *de novo* in IL-1β-tdVSMCs correspond to a family of short AC8 proteins derived from new AC8 splice variants that we have named “E”, “F”, “G” and “H” in accordance with the nomenclature of previously identified variants [24,26]. AC8E-H isoforms are catalytically inactive and act as dominant-negatives by dimerizing with endogenous full-length ACs and retaining them in the rough endoplasmic reticulum (RER), thereby reducing global cAMP production within the cell. The existence of these dominant-negative isoforms may account for an additional, unsuspected degree of cAMP signaling regulation, and reconcile the *de novo* expression of an AC with the transdifferentiation process of VSMCs.

ACCEPTED MANUSCRIPT

ACCEPTED MANUSCRIPT

2. Materials and methods

2.1. Reagents

Dulbecco's modified Eagle's medium (DMEM), type I collagen from calf skin, poly-L-lysine, L-glutamine, penicillin, streptomycin, thapsigargin, isoproterenol and 3-isobutyl-1-methylxanthine (IBMX) were purchased from Sigma-Aldrich, Saint Quentin Fallavier, France. We obtained fetal calf serum (FCS) and collagenase from Gibco BRL, Cergy-Pontoise, France and G418 from InvivoGen, San Diego, CA, USA. Elastase and the LightCycler 480 SYBR Green I Master mix were obtained from Roche Diagnostics, Meylan, France. Recombinant human IL-1β was purchased from PeproTech, Neuilly-sur-Seine, France, and forskolin (fsk) was obtained from Tocris Bioscience, Bristol, UK. Opti-MEM, Lipofectamine RNAiMAX, M-MLV reverse transcriptase, oligo(dT) primers, RNaseOUT recombinant ribonuclease inhibitor, NuPAGE LDS sample buffer and polyacrylamide gels were obtained from Invitrogen, Life Technologies, Saint-Aubin, France. We purchased the QIAquick gel extraction kit from Qiagen, Les Ulis, France. FuGENE HD, the ReliaPrep RNA Cell Miniprep System and GoTaq DNA polymerase were purchased from Promega, Charbonnières-les-Bains, France. Control and AC8 small interfering RNAs (siRNAs) were obtained from siTOOLs Biotech GmbH, Planegg, Germany. ArrayScript reverse transcriptase, Platinum SuperFi DNA polymerase, Halt protease inhibitor cocktail, EZ-Link Sulfo-NHS-SS-Biotin and streptavidin agarose resin were obtained from Thermo Fisher Scientific, Villebon sur Yvette, France. We purchased GelRed from Biotium, Fremont, CA, USA and oligonucleotides from Eurofins Genomics, Les Ulis, France. The DC protein assay and the Clarity western ECL substrate were purchased from Bio-Rad, Marnes-la-Coquette, France. Protein G PLUS-Agarose was obtained from Santa Cruz Biotechnology, Inc., Dallas, TX, USA and nitrocellulose membranes were purchased from Amersham, Courtaboeuf, France. N-glycosidase F was obtained from New England Biolabs, Évry, France. We obtained the cAMP - Gs HiRange kit from Cisbio Bioassays, Codolet, France and the Dako fluorescence mounting medium from Dako, Carpinteria, CA, USA.

2.2. Cell culture

Adult male Wistar rats (Janvier Labs, Le Genest-Saint-Isle, France) were ethically sacrificed by an intraperitoneal injection of pentobarbital (300 $mg.kg^{-1}$) and VSMCs were isolated from thoracic aortas as previously described [7], according to European Directive 2010/63/EU and

ACCEPTED MANUSCRIPT

the rules laid down by the university ethics committee. Primary VSMC cultures were subcultured from passages 1 to 3 in culture dishes coated with type I collagen from calf skin. Cells were grown at 37°C, under an atmosphere containing 5% CO_2, in DMEM containing 1 $g.L^{-1}$ glucose, 4 mM L-glutamine, 10% FCS, 100 $U.mL^{-1}$ penicillin, and 100 $\mu g.mL^{-1}$ streptomycin. VSMCs were starved by incubation for 12 h in serum-free DMEM before treatment with IL-1β (10 $ng.mL^{-1}$) for 72 h.

HEK-293 cells were grown at 37°C, under an atmosphere containing 5% CO_2, in DMEM containing 4.5 $g.L^{-1}$ glucose, 4 mM L-glutamine, 5% FCS, 100 $U.mL^{-1}$ penicillin, and 100 $\mu g.mL^{-1}$ streptomycin.

2.3. Transfection

Before transfection with siRNAs, VSMCs at 80% confluence were incubated for 2 h in antibiotic-free DMEM containing 1 $g.L^{-1}$ glucose, 4 mM L-glutamine and 10% FCS. Cells were then transfected by adding 0.25% Lipofectamine RNAiMAX and 5 nM siRNAs diluted in 12.5% final Opti-MEM. Cells were transferred, 24 h after transfection, to starvation (serum-free) medium for 12 h. The AC8 siRNA is a mixture of 30 different siRNAs directed against mRNA regions conserved in all AC8 splice variants (reference sequence: NM_017142.1). The AC8E-H siRNA consists of 6 different siRNAs directed against the E5SS-3SS junction that is present only on AC8E-H mRNAs.

Plasmid transfection was systematically performed with HEK-293 cells at 80% confluence in complete growth medium, in the presence of FuGENE HD and Opti-MEM, according to the information provided in the FuGENE HD Protocol Database (Promega). Cells were systematically used 48 h post-transfection. Stable transfection was performed in the same complete growth medium supplemented with 0.8 $\mu g.mL^{-1}$ G418 antibiotic for one week, and monoclonal cell populations were generated by limiting dilution.

2.4. Cloning strategies

To clone the AC8 splice variants expressed in IL-1β-tdVSMCs, cells were treated with IL-1β (10 $ng.mL^{-1}$) for 72 h and total RNA was extracted with the ReliaPrep RNA Cell Miniprep System. Total RNA (1 µg) was then reverse-transcribed with ArrayScript reverse transcriptase and 2.5 µM oligo(dT) primers. The cDNAs encoding the rat AC8 were amplified with Platinum SuperFi DNA polymerase, using phosphorylated forward and reverse primers (Table S1)

ACCEPTED MANUSCRIPT

binding to the 5'-untranslated region and the 3'-untranslated region of the rat AC8A cDNA (NM_017142.1), respectively. The final PCR products were visualized by electrophoresis in a 1% agarose gel. Amplicons of the expected size were purified with the QIAquick gel extraction kit and blunt-cloned into the EcoRV site of pcDNA3. Positive clones were sequenced and four cDNAs encoding AC8 were identified and named AC8E, F, G and H.

We obtained pcDNA3-VSV by inserting a double-stranded HindIII/KpnI-compatible end oligonucleotide adaptor (Table S1), including the vesicular stomatitis virus glycoprotein tag sequence (VSV), between the HindIII and KpnI restriction sites of pcDNA3. AC8A, AC8E and AC8H coding sequences were amplified by PCR with primers deleting the start codon (Table S1). The purified PCR fragments were inserted between the KpnI and XbaI restriction sites of pcDNA3-VSV to generate plasmids encoding N-terminally VSV-tagged AC8A, AC8E and AC8H.

We generated the HA-AC3-expressing vector by inserting a double-stranded EcoRI/BamHI-compatible end oligonucleotide adaptor (Table S1), including the human influenza hemagglutinin (HA) epitope sequence, in frame with the first 26 coding bases of the rat AC3 sequence (from +3 to +29, including the internal rAC3 BamHI site), in place of the EcoRI/BamHI fragment of pcDNA3-rAC3 (a generous gift from C. Dessauer).

All clones and constructs were sequenced on both strands, by dye-labeling chain-terminator chemistry methods, with an ABI 3730xl DNA Analyzer (Thermo Fisher Scientific, Villebon sur Yvette, France).

2.5. PCR

Total RNA was extracted with the ReliaPrep RNA Cell Miniprep System, according to the manufacturer's protocol. After annealing oligo(dT) primers (1 μM) to template RNAs (0.5-1 μM) at 70°C for 5 min, we initiated primer extension by adding M-MLV reverse transcriptase plus 0.5 mM dNTPs, 1 unit of RNaseOUT recombinant ribonuclease inhibitor and 20 mM DTT, and incubated the reaction mixture for a further 60 min at 37°C.

Quantitative PCR was performed with a LightCycler 480 instrument as described previously [28]. The forward and reverse primers used for selective amplification of the cDNAs encoding rat cyclophilin A, ACs and C-C motif chemokine ligand 3 (CCL3) are presented in Table S1. Real-time quantitative PCR data are presented as the amount of each target mRNA relative to the amount of mRNAs for the cyclophilin A housekeeping reference gene.

ACCEPTED MANUSCRIPT

For the relative quantification of the various AC8 transcripts, cDNAs from rat brain and VSMCs (equivalent to 50 ng of total RNA) were amplified in a Prime Full Size Thermal Cycler (Techne, Stone, UK) with 1.25 U of GoTaq DNA polymerase, 1.5 mM $MgCl_2$, 0.2 mM of each dNTP, and 0.5 µM of forward and reverse primers. Equal loading of the reverse-transcribed mRNAs was controlled by amplifying GAPDH cDNAs in each sample. Primer pairs for RT-PCR analysis were tested for self-complementarity, dimer formation and melting temperature with Serial Cloner 2-6-1 software. PCR was performed with the following thermal settings: denaturation and enzyme activation at 95°C for 2 min, with 25 to 33 cycles of 95°C for 1 min, 58 to 64°C for 1 min, and 72°C for 1 min, followed by a final extension at 72°C for 5 min. The sizes of the amplified fragments were determined by GelRed staining after electrophoresis in a 2% agarose gel. The PCR fragments were visualized with a E-BOX VX5 digital image processor (Vilber Lourmat, Collégien, France) and signal intensity was determined with Image J software. The forward and reverse primers used for selective amplification of the AC8 and GAPDH cDNAs are presented in Table S1.

2.6. Preparation of cell lysates

HEK-293 cells were washed with ice-cold phosphate-buffered saline (PBS), scraped into RIPA lysis buffer (25 mM Tris–HCl, pH 7.5, 150 mM NaCl, 1% NP40, 1% sodium deoxycholate, 0.1% SDS, Halt protease inhibitor cocktail) and subjected to three five-second bursts of sonication with a Sonifier 150 (Branson Ultrasonics, Danbury, CT, USA). The resulting cell lysates were briefly incubated on a rotating wheel for 15 min at 4°C and then cleared by centrifugation (13,000 x *g* for 15 min at 4°C). Protein concentrations were determined with the DC protein assay. Proteins were then mixed with the NuPAGE LDS sample buffer and denatured for 1 h at 37°C before SDS-PAGE analysis.

When indicated, whole-cell lysates were treated with N-glycosidase F before electrophoresis. Briefly, proteins (20 µg) were denatured by heating at 100°C for 10 min in 0.5% SDS and 40 mM DTT. Denatured proteins were incubated with 500 units of N-glycosidase F or the same volume of 50% glycerol (controls) in 20 mM Tris-HCl pH 7.5, 50 mM NaCl, 5 mM EDTA and 1% NP-40 for 1 h at 37°C. Proteins were then mixed with the NuPAGE LDS sample buffer and incubated for 5 min at 100°C before SDS-PAGE analysis.

2.7. Subcellular fractionation

ACCEPTED MANUSCRIPT

HEK-293 cells grown in 10-cm dishes were washed with ice-cold PBS and lysed by passing 10 times through a 26-gauge needle in fractionation (F) buffer containing 20 mM HEPES pH 7.4, 250 mM sucrose, 10 mM KCl, 1.5 mM $MgCl_2$, 1 mM EDTA, 1 mM EGTA, 1 mM DTT and Halt protease inhibitor cocktail. The lysate was first centrifuged at 600 x *g* for 10 min. The supernatant (supernatant 1) was then centrifuged at 10,000 x *g* for 15 min to isolate the heavy membrane pellet. The resulting supernatant 2 was centrifuged at 100,000 x *g* for 1 h in an Optima MAX-XP ultracentrifuge (Beckman Coulter, Brea, CA, USA) to separate the light membrane pellet from the cytoplasmic fraction. The heavy and light membrane pellets were then resuspended in F buffer, passed through a 26-gauge needle 10 times and recentrifuged at the speeds indicated above. The resulting pellets, corresponding to the heavy membrane and light membrane fractions, were washed twice with PBS and resuspended in a final PBS buffer supplemented with 2% SDS.

2.8. Cell surface biotinylation

HEK-293 cells grown in 6-cm dishes were biotinylated in the presence of PBS+ (0.1 mM $CaCl_2$, 1 mM $MgCl_2$, pH 8.0) supplemented with 1.5 $mg.mL^{-1}$ sulfosuccinimidyl-2-(biotinamido) ethyl-1,3-dithiopropionate (EZ-Link Sulfo-NHS-SS-Biotin) for 45 min at 4°C. Cells were then incubated for another 45 min at 4°C with a quenching solution containing PBS+ supplemented with 100 mM glycine. Cells were washed with PBS and solubilized in lysis buffer (20 mM Tris HCl pH 7.4, 2 mM EDTA, 2 mM EGTA, 0.1% SDS, 1% Triton, Halt protease inhibitor cocktail). Biotinylated proteins were precipitated with streptavidin agarose resin suspended in 50 mM Tris HCl pH 7.4, 100 mM NaCl, 50 mM EDTA, Halt protease inhibitor cocktail. Precipitated proteins were resuspended in 2X NuPAGE LDS sample buffer, denatured for 30 min at 37°C and subjected to western blot.

2.9. Co-immunoprecipitation

HEK-293 cells grown in 10-cm dishes were washed with ice-cold PBS and lysed in 1 mL of solubilization (S) buffer (50 mM Tris pH 7.4, 1 mM EDTA, 150 mM NaCl, 0.3% (v/v) NP40, and Halt protease inhibitor cocktail). After incubation for 15 min on a rotating wheel, the cell suspension was passed 10 times through a 21-gauge needle and centrifuged at 10,000 x *g* for 10 min. The supernatant was then harvested, incubated on a rotating wheel for 1 h with 5 µl of anti-HA or anti-VSV antibody (Table S2) and then incubated overnight with 40 µL of 50%

ACCEPTED MANUSCRIPT

Protein G PLUS-Agarose bead slurry. Beads were washed five times in S buffer and complexes were eluted in 2X NuPAGE LDS sample buffer. The final eluate was vortexed vigorously and incubated for 1 h at 37°C before western blot analysis.

2.10. Western blot

Proteins were subjected to SDS-PAGE and transferred onto nitrocellulose membranes. Membranes were blocked by incubation for 1 h at room temperature with Tris-buffered saline supplemented with 0.1% Tween 20 and 5% non-fat dried milk. Then, membranes were successively incubated with the primary antibodies indicated in Table S2 and horseradish peroxidase (HRP)-conjugated secondary antibodies. Signals were detected by enhanced chemiluminescence using the Clarity western ECL substrate, on Fujifilm LAS-300 (Fujifilm Medical Systems, Standford, CT, USA). When indicated, we used β-actin detection to control for equal protein loading and transfer efficiency.

2.11. Immunocytochemistry

HEK-293 cells were grown to subconfluence on poly-L-lysine-coated coverslips and fixed by incubation with 4% PFA for 30 min. PFA was then neutralized by incubation for 10 min with 50 mM NH_4Cl at room temperature. Cells were then permeabilized by incubation with 0.2% Triton X-100 in PBS for 5 min. Before immunodetection, non-specific sites were blocked by incubating cells in PBS supplemented with 5% donkey serum, 0.2% Triton X-100. Then, cells were successively incubated with the primary antibodies indicated in (Table S2) and Alexa Fluor conjugated secondary antibodies diluted in PBS supplemented with 5% donkey serum. The coverslips were mounted in Dako fluorescence mounting medium. Images were acquired with a Leica SP5 confocal microscope (Leica Microsystems, Wetzlar, Germany).

2.12. Measurement of cAMP dynamics

Cells on collagen (VSMCs) or poly-L-lysine (HEK-293)-coated coverslips were infected with the $^{T}Epac^{VV}$-encoding adenoviral vector (~100 particles per VSMC) or transfected with the $^{T}Epac^{VV}$-encoding vector (HEK-293) for 24 h. The generation of the $^{T}Epac^{VV}$-encoding adenovirus has been described elsewhere [28]. Coverslips were placed in a microscope chamber continually perfused (2 $mL.min^{-1}$) with a BBS buffer containing 125 mM NaCl, 2 mM $CaCl_2$, 1 mM $MgCl_2$, 1.25 mM NaH_2PO_4, 26 mM $NaHCO_3$, 25 mM glucose, maintained at 32°C and

ACCEPTED MANUSCRIPT

saturated with 95% O_2 - 5% CO_2. Ratiometric analyses were performed as follows: fluorescence was excited with a LED source at 435 nm, and fluorescence emission was monitored with a dichroic mirror (T450LPXR) and alternating emission filters for the donor (HQ480/40) and acceptor (D535/40). Pairs of images were recorded with a Orca-ER CCD camera (Hamamatsu Photonics, Japan), at 20-second intervals. Changes in $[cAMP]_i$ are expressed as the ratio of donor fluorescence (F480) to acceptor fluorescence (F535). The ratios were multiplied by a same constant for all experiments, such that the baseline ratio was 1 in basal conditions. The maximum ratio change (Rmax) was obtained by stimulating cells with 10 μM fsk and 200 μM IBMX. Filters and mirrors were obtained from AHF analysentechnik AG, Tübingen, Germany.

2.13. cAMP accumulation assay

cAMP accumulation in whole-cell lysates was measured with the cAMP - Gs HiRange kit after incubation for 60 minutes with the PDE inhibitor 3-isobutyl-1-methylxanthine (IBMX, 500 μM) and the general AC activator forskolin (fsk, 10 μM), according to the manufacturer's instructions.

2.14. Statistics

All data are presented as the means ± SEM of at least three independent experiments. The statistical significance of differences between groups was assessed with GraphPad Prism 6 (Graphpad Software Inc., La Jolla, CA, USA). The nonparametric two-tailed Mann-Whitney test was used for pairwise comparisons. The nonparametric two-tailed Kruskal-Wallis test and Dunn's post test were used for multiple comparisons. Differences were considered significant if $P < 0.05$.

ACCEPTED MANUSCRIPT

ACCEPTED MANUSCRIPT

3. Results

3.1. The AC8 molecules expressed in IL-1β-transdifferentiated VSMCs belong to a novel family of AC8 isoforms, all lacking the first five transmembrane domains

We previously showed that the *de novo* expression of AC8 is a key feature of rat VSMCs undergoing transdifferentiation (tdVSMCs) in response to IL-1β [7,8,10]. Four different splice variants of AC8, encoding the AC8A-D isoforms, have been identified [24–27]. AC8A is the full-length isoform. AC8B, C and D variants lack exon 11, exon 8 and both these exons, respectively. We cloned the AC8 cDNAs from rat VSMCs stimulated with IL-1β (10 $ng.mL^{-1}$) for 72 hours. All 13 clones sequenced displayed a non-frameshift 414 bp deletion at the end of the exon 1, termed c.538_951del. The non-frameshift deletion stretches from a canonical alternative 5' donor site in exon 1 (E5SS, changing the 3' boundary of exon 1) to the 3' acceptor splice site (3SS) of intron 1. Some cDNAs lack exon 8 and/or exon 11 (Fig. 1A and S1). Thus, IL-1β-tdVSMCs express a new family of four splice variants of the AC8 primary mRNA named AC8E to H: the AC8E mRNA lacks only the end of exon 1, whereas the AC8F, G and H mRNAs also lack exon 8, exon 11, and both these exons, respectively (Fig. 1A).

We then determined the relative abundances of AC8E-H transcripts and AC8A-D messengers (pooled together). We distinguished between these two pools of variants by amplifying cDNAs generated from IL-1β-tdVSMC mRNAs with forward (F) and reverse (R) primers annealing on either side of c.538_951del (Fig. 1B, left), assuming that the AC8E-H PCR products would be 395 bp long whereas the AC8A-D PCR products would be 800 bp long. We used cDNAs from contractile VSMCs and rat brain as negative and positive controls, respectively, for AC8 expression. As expected (Fig. 1B, middle) [29], an intense 800 bp band was detected in brain samples, in which the 395 bp band was barely visible; neither of these two bands was detected in contractile VSMC samples, confirming the lack of AC8 expression in these cells. In IL-1β-tdVSMC samples, the 395 bp PCR products relating to AC8E-H were highly abundant, whereas the 800 bp PCR products corresponding to AC8A-D were barely detectable. Based on a densitometric analysis of fluorescent amplicons, AC8E-H accounted for more than 90% of total AC8 transcripts in IL-1β-tdVSMCs (Fig. 1B, right). Consistently, siRNAs specifically targeting AC8E-H (*i.e.* spanning the E5SS-3SS junction) and siRNAs targeting all AC8 splice variants decreased the expression of C-C motif chemokine ligand 3 (CCL3) and cyclooxygenase-2 (COX-2) to a similar extent (Fig. S2).

ACCEPTED MANUSCRIPT

The relative abundances of AC8E to H variants were determined with forward (F) and reverse (R) primers binding to exons 7 and 12, respectively (Fig. 1C, left and middle). These amounts are expressed as a percent of total AC8E-H mRNAs: 15.5% for AC8E, 18% for AC8F, 30.5% for AC8G and 36% for AC8H in IL-1β-tdVSMCs (Fig. 1C, right). All the AC8E-H transcripts lack the 414 bp region encoding the putative first five transmembrane domains (TM), three extracellular and two intracellular loops of the enzyme (Fig. S1 and S3). The AC8F and AC8G mRNAs additionally lack either exon 8 (198 bp) encoding a 66-amino acid cytoplasmic domain corresponding to almost the entire C1b region, or exon 11 (90 bp) encoding a 30-amino acid extracellular domain corresponding to the TM9-10 loop, with two functional sites for N-linked glycosylation, respectively [30]. AC8H displays all three deletions.

ACCEPTED MANUSCRIPT

ACCEPTED MANUSCRIPT

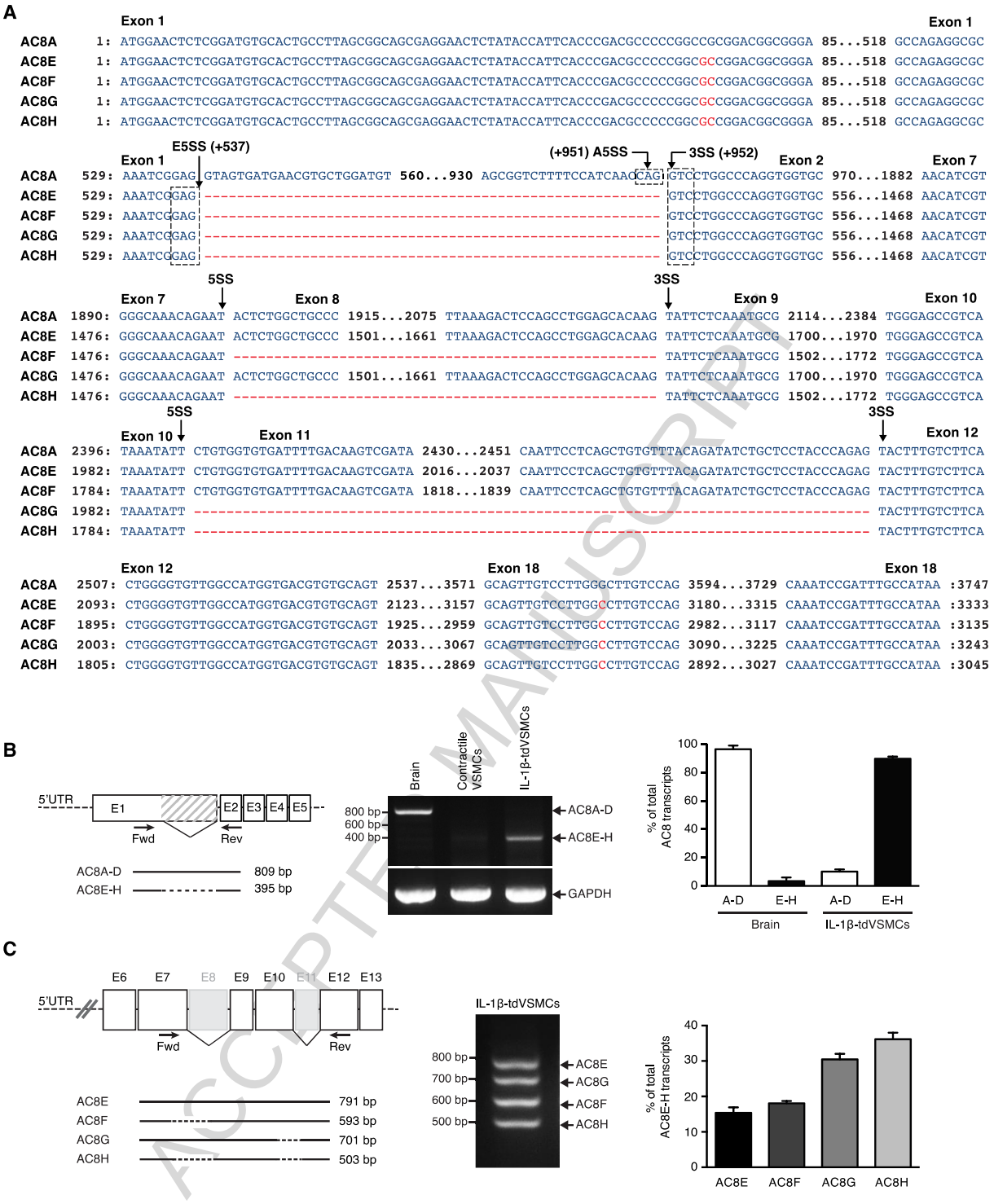

Figure 1 - Four AC8 splice variants are expressed in IL-1β-transdifferentiated VSMCs

A Alignment of the AC8A reference sequence (NM_017142.1) with the AC8E-H coding sequences. Red dotted lines represent the nucleotide regions deleted in AC8E-H variants; black arrows indicate the 5' donor sites (5SS) and the 3' acceptor site (3SS) involved in alternative

ACCEPTED MANUSCRIPT

splicing; AC8E-H polymorphisms relative to the AC8A reference sequence (NM_017142.1) are marked in red.

B Relative abundances of AC8E-H and AC8A-D transcripts in rat brain, contractile VSMCs and IL-1β-tdVSMCs assessed by conventional PCR. Left panel: diagram of the PCR strategy with primers annealing on either side of c.538_951del and expected PCR products. Middle panel: agarose gel of the resulting PCR products. Equal loading of the reverse-transcribed mRNAs was controlled by amplifying GAPDH cDNAs in each sample. Right panel: relative quantification of AC8A-D and AC8E-H mRNAs in brain and IL-1β-tdVSMCs, based on a densitometric analysis of fluorescent amplicons. Results are expressed in % of total AC8 transcripts and represent the means ± SEM of 4 independent experiments.

C Relative abundances of the AC8E to H transcripts in IL-1β-tdVSMCs assessed by conventional PCR. Left panel: diagram of the PCR strategy with forward (F) and reverse (R) primers binding to exons 7 and 12 and expected PCR products. Middle panel: agarose gel of the resulting PCR products. Right panel: relative quantification of AC8E-H mRNAs in IL-1β-tdVSMCs. Results are expressed in % of total AC8E-H transcripts and represent the means ± SEM of 5 independent experiments.

3.2. The *de novo* expression of AC8E-H in IL-1β-transdifferentiated VSMCs downregulates cAMP production

We then investigated a possible change in the dynamics of cAMP production associated with the *de novo* expression of AC8E-H in VSMCs, using the FRET-based biosensor $^{T}Epac^{VV}$ [31]. Rat VSMCs were transdifferentiated by IL-1β treatment (10 ng.mL^{-1}) for 72 hours. Relative changes in $[cAMP]_i$ in response to the AC activator forskolin (fsk, 10 μM) were monitored over time, by calculating the ratio R of donor (F480 nm) to acceptor (F535 nm) fluorescence. cAMP level is reported as a percentage of the maximum ratio change (Rmax), corresponding to saturation of the biosensor. Rmax was systematically determined at the end of the experiment, by adding 200 μM 3-isobutyl-1-methylxanthine (IBMX), a broad-spectrum PDE inhibitor, in the presence of 10 μM fsk. In contractile VSMCs, fsk addition increased the mean fluorescence ratio to 96.9 ± 1.7% of Rmax (Fig. 2A). By contrast, cAMP responses barely reached 53.3 ± 6.6% of Rmax in IL-1β-tdVSMCs. At the start of the experiment, the baseline ratio was similar for contractile VSMCs and IL-1β-tdVSMCs (Fig. S4A). A similar decrease in cAMP responses

ACCEPTED MANUSCRIPT

was observed in IL-1β-tdVSMCs when the experiments were performed with isoproterenol (25 nM), a non-selective β-adrenoceptor agonist (Fig. S5).

We used a siRNA strategy to investigate whether the smaller increase in $[cAMP]_i$ in IL-1β-tdVSMCs was due to the *de novo* expression of AC8E-H (Fig. 2B). As expected, in IL-1β-tdVSMCs transfected with the control siRNA, the response to fsk was similar to that of untransfected IL-1β-tdVSMCs (46.0 ± 6.1 *vs.* 53.3 ± 6.6% of Rmax, Fig. 2A *vs.* Fig. 2B). However, a partial recovery of the cAMP responses was observed in IL-1β-tdVSMCs transfected with the AC8 siRNA: in these cells, fsk increased the fluorescence ratio to a significantly higher level than in IL-1β-tdVSMCs transfected with the control siRNA (65.5 ± 6.7 *vs.* 46.0 ± 6.1% of Rmax, Fig. 2B). Baseline ratios were similar in IL-1β-tdVSMCs transfected with the control siRNA and in IL-1β-tdVSMCs transfected with the AC8 siRNA (Fig. S4B). The efficacy and specificity of the AC8 siRNA were demonstrated by real-time PCR 48 h post-transfection (Fig. S6). Together, these data demonstrate that the *de novo* expression of AC8E-H profoundly affects cAMP dynamics by reducing the increase in $[cAMP]_i$ in IL-1β-tdVSMCs. This reconciles the increased expression of AC8 in atherosclerotic vessels with the reduced cAMP levels required for the pathological proliferation and migration of inflammatory VSMCs.

ACCEPTED MANUSCRIPT

ACCEPTED MANUSCRIPT

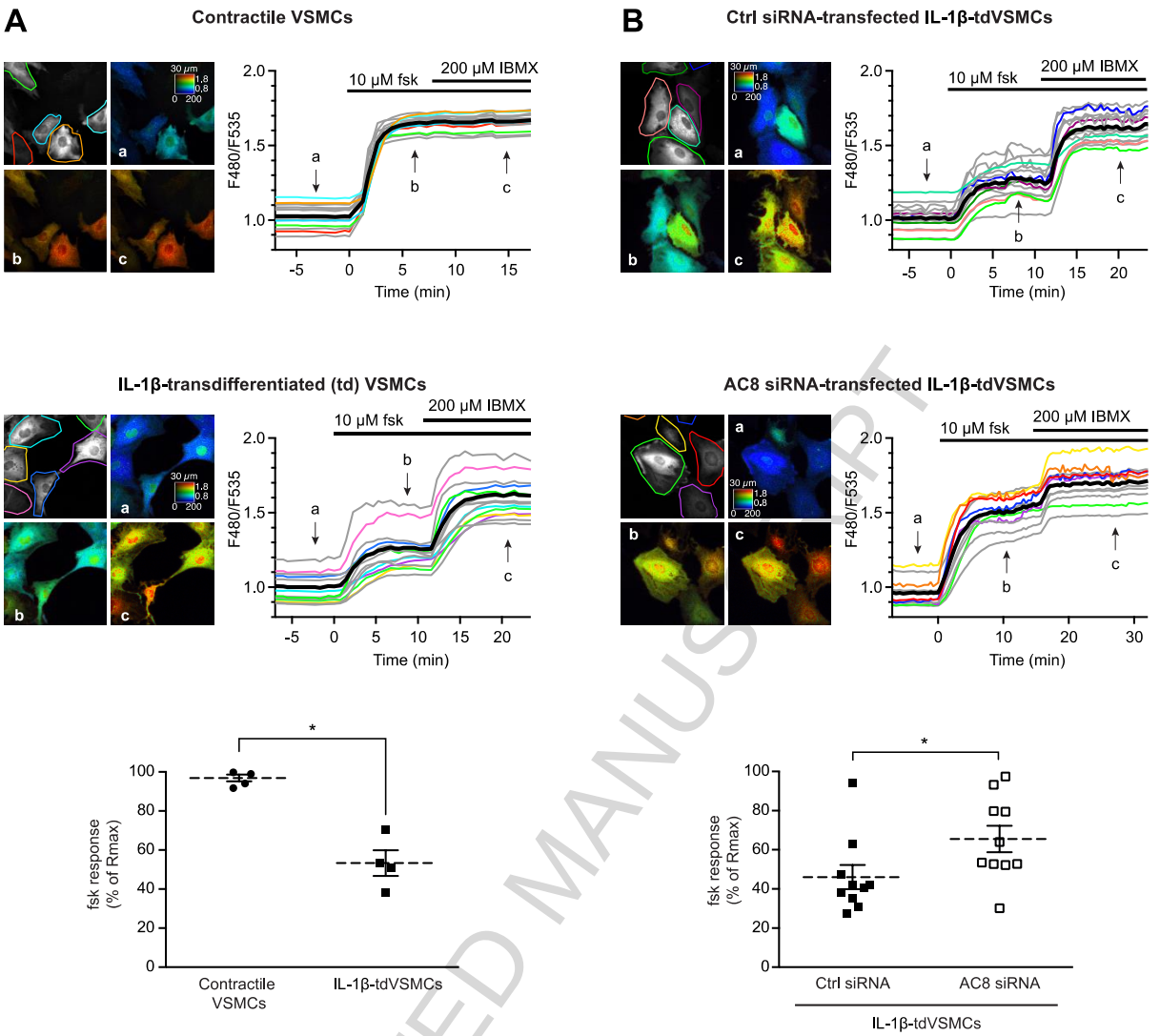

Figure 2 – The *de novo* expression of AC8E-H in IL-1β-transdifferentiated VSMCs reconfigures the dynamics of the cAMP signal

A, **B** Biosensor imaging of relative changes in $[cAMP]_i$ following treatment with fsk (10 µM) in contractile VSMCs *versus* IL-1β-tdVSMCs (**A**) and in Ctrl siRNA- *versus* AC8 siRNA-transfected IL-1β-tdVSMCs (**B**). Left panels: microscopy fields in grayscale (top left) showing biosensor crude fluorescence at 535 nm. The F480/F535 ratio was determined for individual cells, within regions of interest (ROI) delimited with colored contours. The calibration square indicates the range of intensity (in counts/pixel/s) horizontally and the F480/F535 ratio vertically. Pseudocolored images represent the F480/F535 ratio indicating the $[cAMP]_i$ (a) before treatment, (b) during 10 µM fsk stimulation and (c) during the application of fsk (10 µM) + IBMX (200 µM). Right panels: each trace indicates the F480/F535 emission ratio over time in the ROI delimiting each cell. The black line represents the average of all traces. Gray traces

ACCEPTED MANUSCRIPT

correspond to the F480/F535 emission ratio of cells outside the displayed region. Lower panels: dot plot representing the mean values for fsk responses. Results are expressed as a percentage of the maximal ratio change (% of Rmax) determined by the final application of fsk (10 μM) + IBMX (200 μM). Data shown are the means ± SEM of at least $N = 4$ independent experiments performed on $n = 10$ to 20 individual cells. In (**A**), fsk responses were as follows: for contractile VSMCs: 96.9 ± 1.7%, $N = 5$; for IL-1β-tdVSMCs: 53.3 ± 6.6%, $N = 4$, $P = 0.0159$. In (**B**), fsk responses were as follows: for Ctrl siRNA-transfected IL-1β-tdVSMCs: 46.0 ± 6.1%, $N = 10$; for AC8 siRNA-transfected IL-1β-tdVSMCs: 65.5 ± 6.7%, $N = 10$, $P = 0.0288$. Side-by-side comparisons were performed with the Mann-Whitney test for unpaired data. *: $P < 0.05$.

3.3. Expression and localization of AC8E-H isoforms

The lack of the TM9-10 loop with two functional sites for N-linked glycosylation in AC8B reduces its expression relative to that of AC8A and AC8C [24]. Since AC8G and H both miss this N-glycosylated extracellular domain, we next analyzed in western blot the protein expression of AC8E-H from four different clones of stably transfected HEK cells (Fig. 3A). The antibody we used was raised against the C2b terminal domain, a region that remains present in AC8E-H isoforms. AC8E and AC8F clones expressed high protein levels. Consistently with the study of Cali et al. [24], we found that AC8G and AC8H were very poorly expressed.

Subcellular fractionation experiments demonstrated that AC8E-H isoforms still insert into cellular membranes (Fig. 3B). Indeed, AC8E-H and the full-length AC8A mainly concentrated in the heavy membranes fraction and were absent from the cytosolic fraction. Heavy membranes include the plasma, endoplasmic reticulum and mitochondrial membranes, as attested by the levels of markers for these membranes, β1-integrin, calnexin and cyclooxygenase IV (COX IV), respectively, and the absence of β-actin, a cytosolic marker. In AC8A HEK samples (Fig. 3B), the immunoreactive bands between the 180 and 250 kDa molecular mass markers are of the size expected for AC8A monomers; the bands above 300 kDa are compatible with the predicted size of AC8A homodimers. In the samples derived from AC8E-H HEK, bands at or below 130 kDa and those around 300 kDa correspond to the monomeric and dimeric AC8E-H species, respectively (Fig. 3A and 3B). The anti-AC8 antibody does not cross-react with any endogenous AC, as no bands were detected in the control HEK samples (Fig. 3B).

ACCEPTED MANUSCRIPT

Immunocytochemistry showed AC8A at the plasma membrane whereas AC8E-H were intracellular and extranuclear (Fig. 3C). Hence, AC8A but not AC8E was detected when purifying biotinylated cell surface proteins (Fig. 3D). Unfortunately, these results could not be confirmed in IL-1β-tdVSMCs due to the low expression level of endogenous AC8E which, along with the low efficiency of AC8 antibodies, led to insufficient signal-to-noise ratios. AC8E is unlikely targeted to mitochondria since it lacks the characteristic specific sequences (TargetP1.1, WoLF PSORT and Predotar 1.04 software). Consistent with AC8E-H progressing through the RER, the migration profile of AC8E was efficiently altered by the exposure of cell lysates to N-glycosidase F (Fig. S7). Interestingly, the migration patterns of AC8A and AC8E were differently sensitive to N-glycosidase F: whereas AC8A showed a continuum of molecular species indicative of partial deglycosylation, the treatment had a less pronounced effect on AC8E. Thus, AC8E likely possesses less diversified N-glycans motifs, in line with AC8E-H isoforms being, to some extent, stuck in the RER during the maturation process. In addition to demonstrating that AC8E and AC8F are the two most strongly expressed isoforms, these results indicate that AC8E-H are all retained in the RER during the maturation process and form intermolecular dimers.

ACCEPTED MANUSCRIPT

ACCEPTED MANUSCRIPT

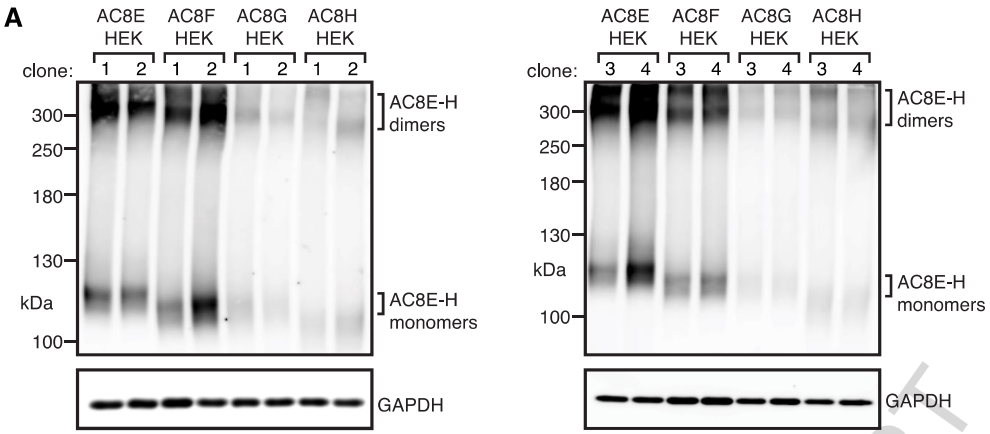

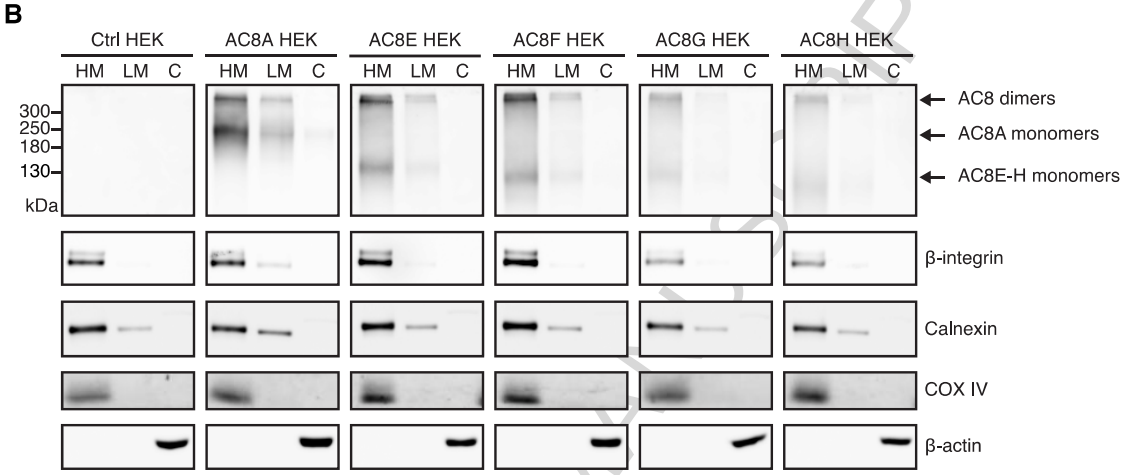

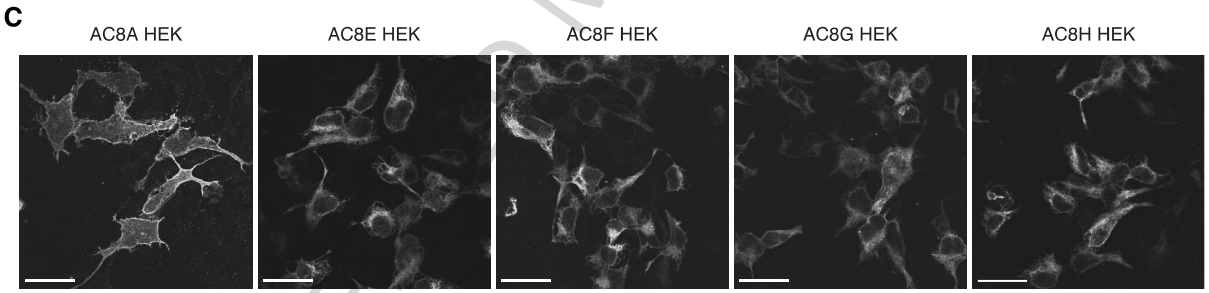

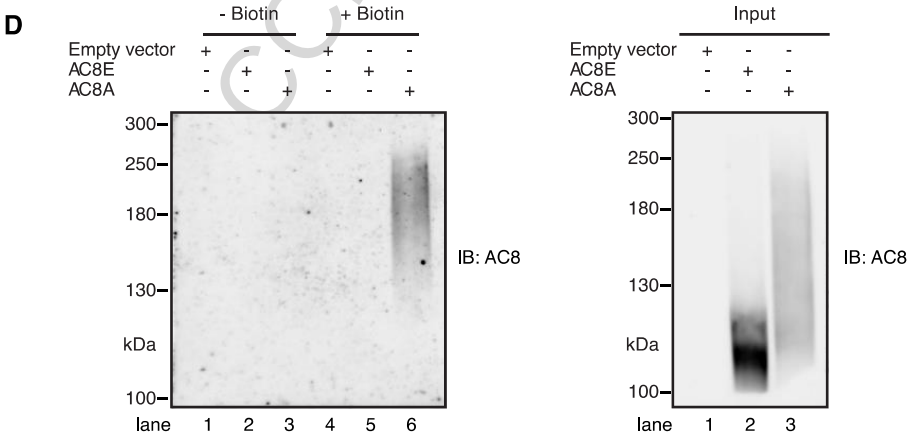

ACCEPTED MANUSCRIPT

Figure 3 - Expression and localization of AC8E-H isoforms

A Western blot showing the stable expression of AC8E, F, G and H in HEK-293 cells. For each construct, four independent clones, numbered 1 to 4, were analyzed.

B Western blot showing the subcellular distribution of AC8A and AC8E-H in heavy membranes (HM), light membranes (LM) and the cytosol (C). β-integrin, calnexin, cyclooxygenase IV (COX IV), and β-actin are markers of the plasma, rough endoplasmic reticulum and mitochondrial membranes and the cytosol, respectively.

C Immunostaining showing the subcellular distribution of AC8A and AC8E-H in HEK-293 cells. Slides were analyzed with a Leica SP5 confocal microscope (63x). Scale bar = 50 μm.

D Western blot analysis of cell surface biotinylated proteins purified from HEK-293 cells transfected with the empty vector or with AC8E- or AC8A-encoding plasmids and inputs. Right panel samples include non- or partially glycosylated AC8As of low molecular weight that are absent from the left panel samples, which only contain mature and fully glycosylated AC8As from the plasma membrane.

Data information: In (**A**-**D**), the western blot and immunofluorescence images shown are representative of at least 3 independent experiments. All AC8 immunodetections were performed with the anti-AC8 (sc-1967) antibody.

3.4. The AC8E-F isoforms are catalytically dead and lower intracellular cAMP concentration

Consistently, only the expression of AC8E and AC8F in HEK cells significantly limits the increase in $[cAMP]_i$ in response to fsk as compared to pcDNA (control)-transfected cells (Fig. 4A). Indeed, the mean fluorescence ratio was 51.1 ± 4.1% and 57.2 ± 2.8% of Rmax in AC8E- and AC8F-transfected cells, respectively, whereas in control HEK cells or in AC8G- and AC8H-expressing cells it reached 87.8 ± 6.1%, 75.5 ± 2.5% and 76.6 ± 4.0% of Rmax, respectively. In AC8A-expressing HEK cells, fsk alone leads to biosensor saturation (101.0 ± 0.6% of Rmax); the basal ratio in AC8A HEK was higher than that in control HEK and AC8E-H HEK, consistent with the overexpression of AC8A increasing basal and induced cAMP production.

As shown previously [32], AC8A is activated by capacitative calcium entry (CCE). We next passively depleted calcium stores with the SERCA inhibitor thapsigargin (500 nM) in the

ACCEPTED MANUSCRIPT

absence of extracellular calcium (1 mM EGTA), and AC activity was jump-started with a low dose of fsk (10 nM). The addition of extracellular calcium (2 mM $CaCl_2$) led to CCE, which increased intracellular cAMP levels in AC8A- but not in control and AC8E-expressing cells (Fig. 4B). This additional experiment shows that AC8E does not exhibit the typical calcium-activated cyclase activity of AC8A. Overall, these results demonstrate that the c.538_951 deletion, despite lying outside the catalytic domains, kills the enzymatic activity of AC8E-H while retaining the ability to lower cAMP responses in AC8E and AC8F.

ACCEPTED MANUSCRIPT

ACCEPTED MANUSCRIPT

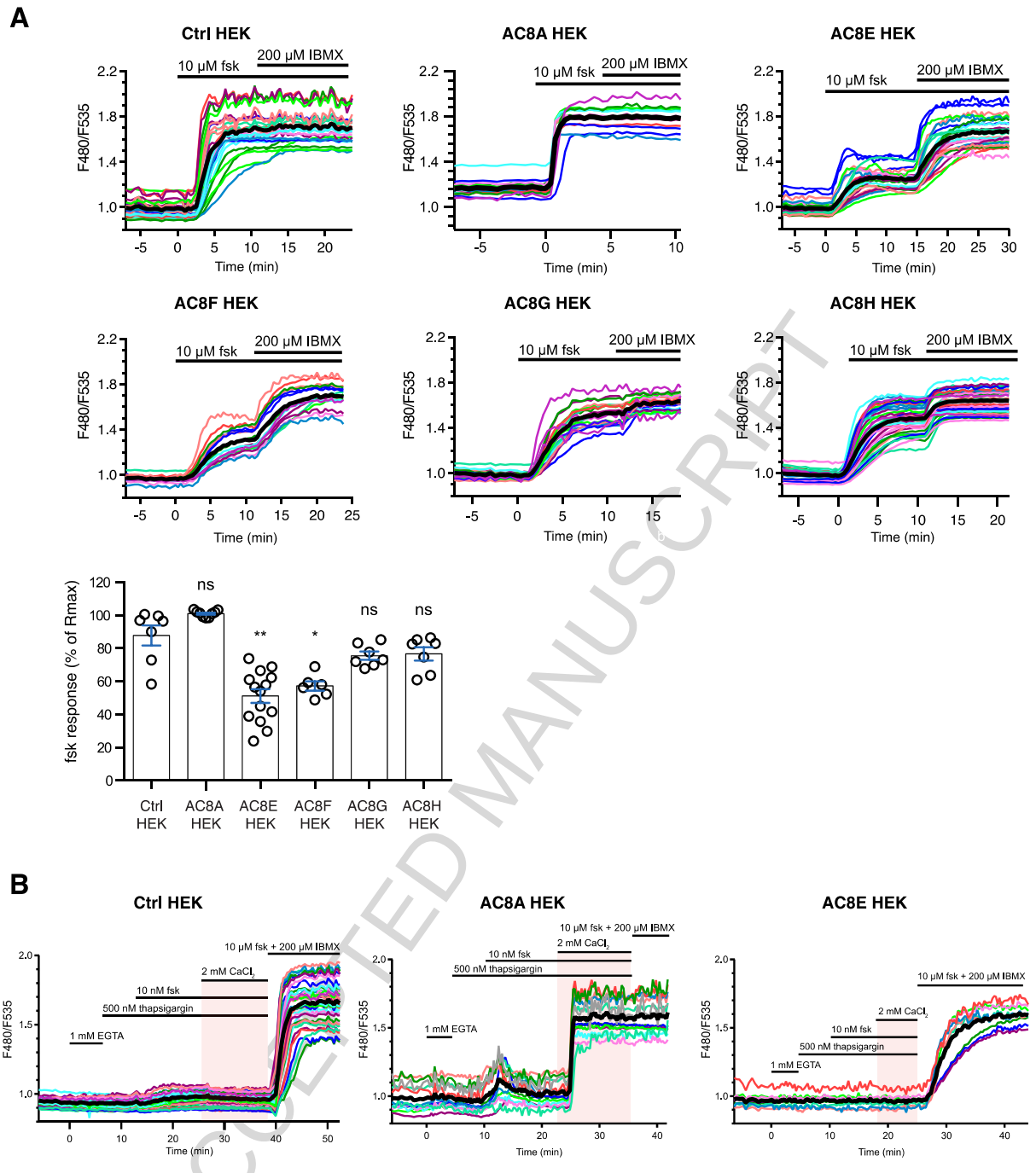

Figure 4 - The AC8E-F isoforms are inactive and prevent increases in cellular cAMP

A Biosensor imaging of relative changes in $[cAMP]_i$ following treatment with fsk (10 µM), in control HEK clones and in clones stably expressing AC8A or AC8E-H. The final application of fsk (10 µM) together with IBMX (200 µM) determined the maximal ratio change. Upper panels: each trace indicates the F480/F535 emission ratio over time in individual cells. The black line represents the average of all traces. Lower panel: dot plot and bars representing

ACCEPTED MANUSCRIPT

the mean values for fsk responses. Results are expressed as a percentage of the maximal ratio change (% of Rmax). Data shown are the means ± SEM of at least N = 6 independent experiments performed on independent clones. For each independent experiment, values represent the mean of n = 10 to 20 individual cells. Fsk responses were as follows: for control HEK: 87.8 ± 6.1%, N = 7; for AC8A HEK: 101.0 ± 0.6%, N = 9, P = 0.6888; for AC8E HEK: 51.1 ± 4.1%, N = 14, P = 0.0030; for AC8F HEK: 57.2 ± 2.8%, N = 6, P = 0.0366, for AC8G HEK: 75.5 ± 2.5%, N = 7, P > 0.9999; for AC8H HEK: 76.6 ± 4.0%, N = 7, P > 0.9999. Multiple comparisons to the control condition were performed with the Kruskal-Wallis test for unpaired data and Dunn's post test. **: P < 0.01, *: P < 0.05, ns: not significant.

B Biosensor imaging of relative changes in $[cAMP]_i$ in response to capacitive calcium entry in control HEK, AC8A HEK and AC8E HEK. The final application of fsk (10 µM) together with IBMX (200 µM) determined the maximal ratio change. Each trace indicates the F480/F535 emission ratio over time in each cell. The black line represents the average of all traces. Data shown are representative of N = 3 independent experiments performed on n = 10 to 20 individual cells.

3.5. AC8E has a dominant-negative effect on endogenous AC activity

We hypothesized that AC8E-F expression reduced cAMP synthesis. We tested this hypothesis by focusing on AC8E as it displays the minimal deletion conferring the ability to restrain increases in $[cAMP]_i$. To do so, we monitored the speed of cAMP synthesis with the FRET-based biosensor $^{T}Epac^{VV}$ by stimulating ACs with a low dose of fsk (1 µM) while blocking PDEs with IBMX (200 µM) (Fig. 5A, upper and middle panels). The ratio increase depends on the buffering effect of the biosensor on cAMP, and a slower onset is expected when the biosensor is present at a higher concentration. Therefore, for each cell, we plotted the slope at the origin of the ratio increase as a function of fluorescence intensity, used as a proxy for biosensor concentration. Regardless of fluorescence intensity, the initial slope of the ratio curve was shallower in AC8E HEK than in control HEK for a same amount of biosensor (Fig. 5A, lower panel). In contrast and as expected, cells expressing AC8A showed a dramatically fast response onset. Similar results were obtained when performing cAMP accumulation assays in whole-cell lysates. AC8E significantly downregulated, by more than three times, whereas AC8A increased, by the same factor, the accumulation of cAMP after a 60-minute period of incubation with fsk (10 µM) plus IBMX (500 µM) as compared to control HEK cells (Fig. 5B).

ACCEPTED MANUSCRIPT

Altogether, these data demonstrate that the inactive AC8E isoform acts as a dominant-negative on endogenous AC activity.

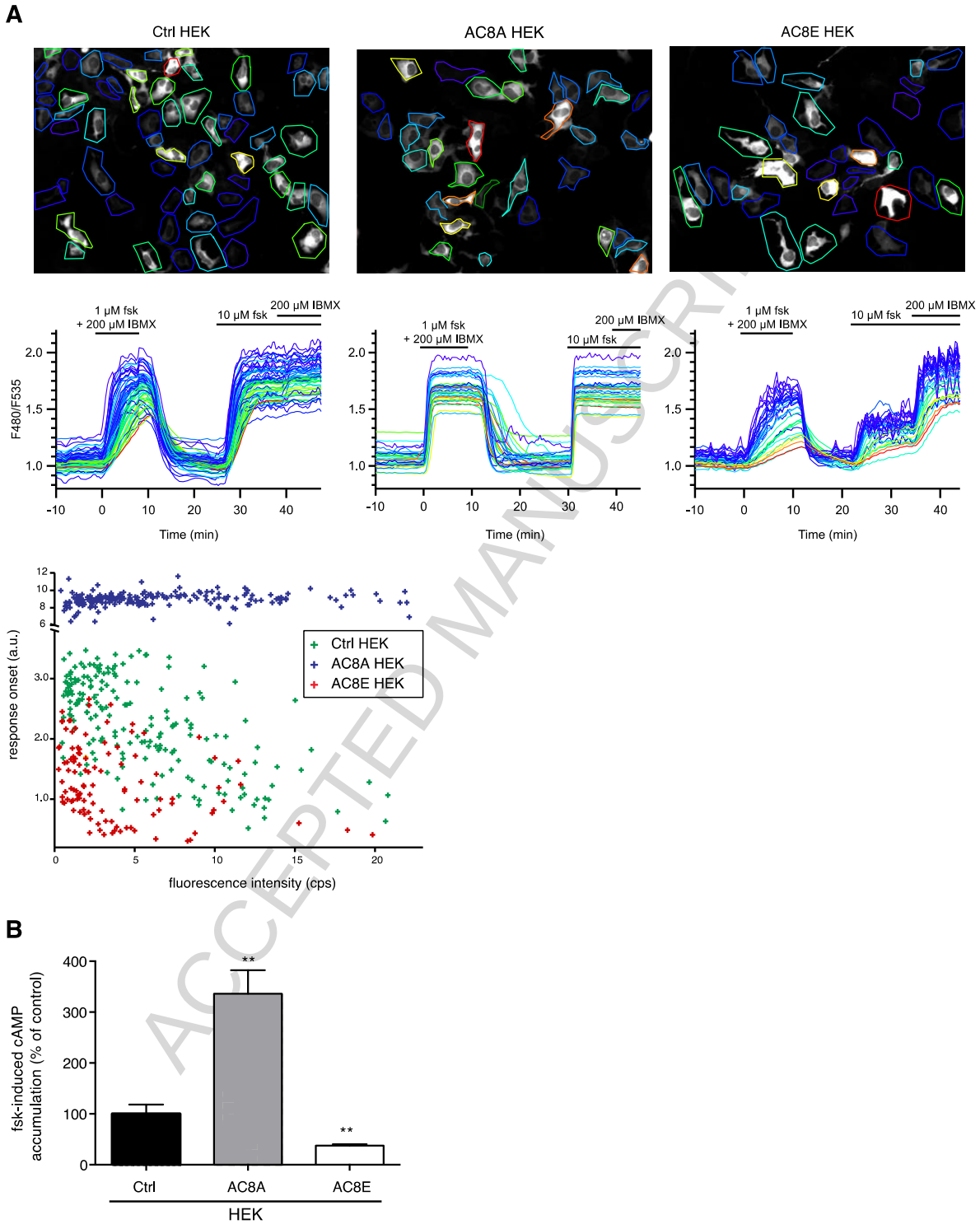

Figure 5 - AC8E expression reduces cAMP production

ACCEPTED MANUSCRIPT

A Changes in $[cAMP]_i$ monitored with $^{T}Epac^{VV}$ in control (pcDNA3-transfected) HEK cells (left) or clones stably expressing AC8A (middle) or AC8E (right). A fast perfusion system was used to apply a low concentration of fsk (1 µM) to activate ACs moderately, in the presence of IBMX (200 µM), to block cAMP degradation by PDEs. After recovery, the final application of fsk (10 µM) together with IBMX (200 µM) determined the maximal ratio change. Upper panels: for each cell, biosensor concentration was estimated by measuring the intensity of the brightest 10% of the pixels within the region of interest. The color code of each ROI reflects biosensor concentration: from blue (low) to red (high). Middle panels: traces indicating the F480/F535 emission ratio over time in the ROI delimiting each cell. Lower panel: onset slope of the fluorescence ratio for each cell plotted against fluorescence intensity (cps) reflecting biosensor expression level. Results of 3 independent experiments are shown.

B cAMP accumulation assays on HEK cells transfected with empty vector (control), AC8A- or AC8E-encoding vector. Results are expressed in % of control and the means ± SEM of 5 independent experiments are shown. Values were as follows: for AC8A HEK: 336.2 ± 46.5%, $P = 0.0079$; for AC8E HEK: 37.8 ± 2.6%, $P = 0.0079$. Side-by-side comparisons were performed with the Mann-Whitney test for unpaired data. **: $P < 0.01$.

3.6. The dominant-negative effect of AC8E combines with direct AC interaction and the blocking of functional AC trafficking

Previous studies have shown that heteromeric complexes assemble between full-length ACs and engineered deletion mutants [33,34]. We next explored whether the dominant-negative AC8E isoform directly influenced AC activity through heterodimer formation. We first assessed the ability of AC8E to interact with AC3, a major AC isoform expressed in VSMCs [4]. HEK cells were transfected with the VSV-tagged AC8E vector or the HA-tagged AC3 vector or both (Fig. 6A), and the interaction between these two proteins was assessed by co-immunoprecipitation. On western blots (Fig. 6B, upper left), after immunoprecipitation of the VSV-tagged AC8E, we detected an immunoreactive band with the anti-HA antibody above 270 kDa in samples from cells transfected with both the VSV- and HA-tagged constructs (lane 4). It corresponds to AC heterodimers containing glycosylated AC3 molecules. No bands were observed in the corresponding negative controls [cells transfected with either VSV-AC8E (lane 3) or HA-AC3 (lane 2) constructs or with the empty vector alone (lane 1)]. As expected, the anti-VSV antibody gave a similar pattern (Fig. 6B, lower left, lanes 3 and 4). Reverse co-

ACCEPTED MANUSCRIPT

immunoprecipitation with the anti-HA antibody for precipitation and the anti-VSV antibody for immunoblotting was just as effective (Fig. 6B, upper right).

This physical interaction translated into significantly lower levels of cAMP synthesis in response to fsk in cells co-expressing AC3 and AC8E than in cells expressing AC3 only (Fig. 6C, 4 *vs.* 3). Again, the expression of AC8E alone decreased the fsk-induced production of cAMP observed in pcDNA3 (control)-transfected cells (Fig. 6C, 2 *vs.* 1).

In addition, HA-AC3 was clearly present within the cell when co-expressed with VSV-AC8E, whereas it reached the plasma membrane when expressed with VSV-AC8A (Fig. 6D). The Pearson's colocalization coefficients with Costes'automatic thresholding (Fiji software Coloc2 plugin) were r = 0.86 for AC8A/AC3 and r = 0.84 for AC8E/AC3. The mis-targeting of endogenous AC3 in IL-1β-tdVSMCs could not be clearly evidenced by immunocytochemistry due to the low expression level of AC3 and the low efficiency of AC3 antibodies leading to insufficient signal-to-noise ratios (Fig. S8).

Overall, these data demonstrate a dominant-negative effect of AC8E on AC3 function associated with a physical interaction between these two proteins, and they suggest that the AC8E-dependent decrease in cAMP synthesis is due to a loss of AC trafficking to the plasma membrane.

ACCEPTED MANUSCRIPT

ACCEPTED MANUSCRIPT

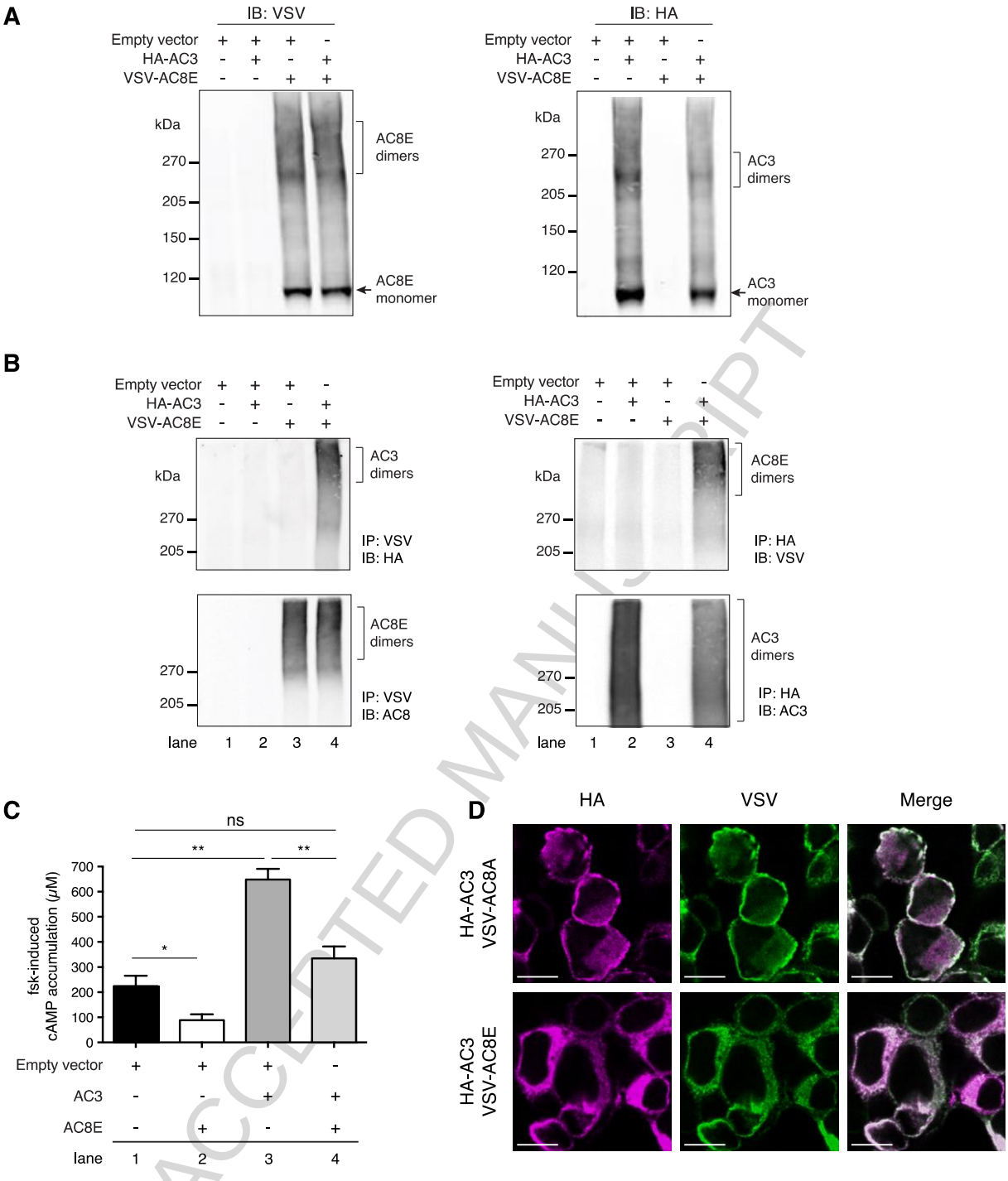

Figure 6 - AC8E heterodimerizes with AC3 and inhibits AC activity

A Western blots showing AC8E (left panel) and AC3 (right panel) levels in HEK-293 cells transiently expressing VSV-AC8E and/or HA-AC3, probed with anti-VSV and anti-HA antibodies.

ACCEPTED MANUSCRIPT

B Western blots showing co-immunoprecipitation results. Immunoprecipitations (IPs) were performed with anti-VSV (left panel) and anti-HA (right panel) antibodies. Immunoblots (IBs) were performed with anti-AC8 (sc-1967) or anti-VSV antibodies to detect AC8E, and with anti-AC3 (sc-588) or anti-HA antibodies to detect AC3.

C cAMP accumulation assays on HEK cells transfected with empty vector and/or AC8E-encoding vector and/or or AC3-encoding vector, after 60 min of treatment with fsk (10 µM) plus IBMX (500 µM). Results are expressed in µM and represent the means ± SEM of 5 independent experiments. Values were as follows: for empty vector-transfected HEK: 224.4 ± 41.3 µM; for AC8E-expressing HEK: 88.9 ± 23.2 µM, $P = 0.0159$; for AC3-expressing HEK: 648.4 ± 42.7 µM, $P = 0.0079$; for AC8E/AC3-expressing HEK: 334.5 ± 47.5 µM, $P = 0.0952$ when compared to control cells and $P = 0.0079$ when compared to AC3-expressing cells. Side-by-side comparisons were performed with the nonparametric Mann-Whitney test for unpaired data. **: $P < 0.01$, *: $P < 0.05$, ns: not significant.

D Immunostaining of HEK-293 cells transfected with plasmids encoding HA-tagged AC3 and VSV-tagged AC8A or AC8E. Detections were performed with the anti-HA and anti-VSV antibodies. Confocal images were acquired with a Leica SP5 confocal microscope (63x). Scale bar = 25 µm.

Data information: In (**A**), (**B**) and (**D**), the western blot and immunofluorescence images shown are representative of at least 3 independent experiments.

ACCEPTED MANUSCRIPT

ACCEPTED MANUSCRIPT

4. Discussion

The transdifferentiation process of medial VSMCs, which allows them to proliferate and migrate towards the intima, is a major cause of atherosclerosis and post-angioplasty restenosis. It has become clear that the contribution of VSMCs to atherosclerotic lesions has been greatly underestimated, because these cells may express macrophage, mesenchymal stem cell and/or myofibroblast markers in lesions [35]. Identification of the molecular mechanisms and entities driving changes in VSMC phenotype is therefore crucial for future drug development programs. Increases in intracellular cAMP concentration inhibit the proliferation and migration of mouse, rat and human VSMCs [12–18], thereby exerting a potent vasculoprotective influence [20–23]. In line with this, several studies have demonstrated that VSMCs undergoing transdifferentiation deploy strategies of cellular desensitization to cAMP signaling, including cAMP hydrolysis by PDEs [20,36–39] and cAMP extrusion by MRPs [23]. The importance of these mechanisms in counteracting the vasculoprotective influence of cAMP is underlined by the fact that PDE inhibitors already moved to human clinical trials and showed positive outcomes on post-angioplasty restenosis [40] and progression of atherosclerosis lesions in patients with type II diabetes [41].

We show here that the IL-1β-dependent transdifferentiation of VSMCs is associated with the *de novo* expression of a new family (the E-H family) of AC8 isoforms. These isoforms are catalytically inactive and have dominant-negative effects, decreasing total cAMP production. The inhibitory effect of AC8E on AC activity is accompanied by the formation of heterodimers between functional ACs and AC8E. The *de novo* expression of AC8E-H in VSMCs is a novel mechanism of cAMP signaling inhibition complementary to those involving PDEs and MRPs. In our experiments, the induction of PDEs and/or MRPs in IL-1β-tdVSMCs could also explain why silencing of AC8 expression did not completely restore the cAMP responses to fsk as compared to contractile VSMCs (Fig. 1).

The lack of enzymatic activity of AC8E-H is consistent with the notion that the C1/C2 interaction forming the catalytic site is not the only one interaction required for cyclase activity, instead being promoted by an intramolecular interaction between intact M1 and M2 transmembrane cassettes [42,43]. The need of this intramolecular interaction also accounts for improper transfer of AC8E-H isoforms towards the plasma membrane [42].

ACCEPTED MANUSCRIPT

AC molecules within homo- and heterodimers of ACs cross-regulate each other. This is well illustrated by *i)* the work of Baragli et al., showing that AC2 and 5 assemble *in vivo* and exhibit enhanced cyclase activity as compared to AC2/AC2 or AC5/AC5 homodimers [44], *ii)* the study of Gu et al., demonstrating that the co-expression of a full-length AC8 together with an inactive engineered mutant (lacking part of the catalytic C1 domain) suppresses its activity [34]. Therefore, the negative regulation of cAMP synthesis by AC8E-F in IL-1β-tdVSMCs is likely due to the ability of these isoforms to form complexes with endogenous full-length ACs. The findings of previous mutagenesis studies suggest that the region involved is the second transmembrane (M2) cassette [34,42]. The M2 hydrophobic cassette of AC8 contains seven SmxxxSm motifs (where Sm is a small residue: Gly, Ala, Ser or Thr) that have been proposed to drive TM helix dimerization in multi-pass proteins [45]. VSMCs mainly express AC3, 5 and 6 [4,9], all of which being capable of forming heterodimers with AC8 (Fig. 6B; [34]). Taking this supplementary information into account, we further propose that AC8E-F inhibit cAMP synthesis within IL-1β-tdVSMCs by acting on AC isoforms 3, 5 and 6.

The theoretical molecular weights of non-glycosylated monomeric AC8E-H range from only 114 to 125 kDa (SerialCloner software). We demonstrated that AC8E-H co-immunoprecipitate endogenous AKAP79 in HEK cells (Fig. S9). AKAP79 binds to the N-terminus of AC8A [46], which also interacts with calmodulin [47], Orai1 [48], PP2A [49] and the actin cytoskeleton [50]. Based on that and on additional studies assuming the existence of ACs oligomers [51,52], we suggest that the bands detected above 300 kDa in Fig. 3 and Fig. 6 correspond to multimeric complexes including more than two AC molecules and/or additional protein partners. A single molecule of AC8E-H interacting with more than one molecule of functional AC may explain why AC8E-F robustly decrease cAMP responses despite a relatively low expression level in IL-1β-tdVSMCs.

Intact M1 and M2 cassettes within a single unit are essential for the correct translocation of AC8A to the plasma membrane (Fig. 3C and 3D; [42]). The overall decrease in cAMP production may, therefore, be due to AC8E-H isoforms retaining full length ACs in the RER. Several lines of evidence suggest that this is probably the case: *i)* AC3 was excluded from the plasma membrane when co-expressed with AC8E (Fig. 6D); *ii)* Ding and collaborators have demonstrated that a truncated form of AC6, similar to the AC8E-H isoforms in the sense that it also lacks one of the two membrane cassettes, prevents full-length AC6 molecules from reaching the plasma membrane [33]. The RER is the seat of protein quality control, addressing

ACCEPTED MANUSCRIPT

misfolded proteins to the ubiquitin-proteasome pathway for degradation. We therefore hypothesize that the lower levels of cAMP production observed in AC8E-expressing cells might be due to the degradation of AC dimers *via* the ER-associated protein degradation (ERAD) system. This could partly explain our inability to detect endogenous AC8E-H proteins in IL-1β-tdVSMCs. In favor of that assumption, the truncated form of AC6 mentioned by Ding and collaborators not only alters the trafficking of full-length AC molecules but also decreases their protein expression level. Such process would amount to a hijacking of the RER protein quality control mechanism from its original purpose, as it would prevent the trafficking of normal proteins to the plasma membrane. Together with alternative splicing, this may constitute a new type of mechanism for regulating protein levels and/or signaling in cells. Although such a regulatory mechanism has never been described before, a role of alternative RNA processing in specifying the post-endocytic sorting of G-protein-coupled receptors has already been established [53].

Our finding that AC8E is N-glycosylated suggests that the two unique functional glycosylation sites of the TM9-10 loop are located within the RER lumen during protein processing (Fig. S7). According to the charge balance rule [54,55], the net charge difference of the 15 amino acids surrounding each end of a transmembrane domain determines its orientation in the lipid bilayer, with the most positive neighboring region facing the cytosol. It has also been shown that *i)* predictive transmembrane domains with a low hydrophobicity may become extramembrane domains and *ii)* highly hydrophobic transmembrane domains stabilize neighboring transmembrane domains of low hydrophobicity [56]. From the charge balance rule, the glycosylation status and the hydrophobic profile of AC8E, one can assume that the remaining sixth transmembrane domain of the M1 cassette relocates to the cytosol and that the M2 cassette anchors to the RER membrane in the same orientation as AC8A. This is even more likely foreseen due to the fact that VSV-tagged AC8E molecules pulled-down endogenous AKAP79 in co-immunoprecipitation experiments, a cytosolic protein known to interact with the N-terminus of AC8A (Fig. S9). Based on that, and consistently with the study of Gu et al. [34], the whole N-terminus/TM6/C1 region of AC8E-H isoforms may be close enough (< 5 nm) to inhibit their AC partners whether by direct interaction or by causing steric hindrance.

The *de novo* expression of AC8E-H in IL-1β-tdVSMCs likely results from both transcriptional activation and splicing regulation. We suggest that the IL-1β-induced activation of the AC8 promoter is primarily cAMP-dependent. This assumption is based on the facts that only IL-1β

ACCEPTED MANUSCRIPT

-as opposed to TNF-α and IFN-γ- induces the *de novo* expression of AC8 (unpublished data) along with an increase in intracellular cAMP levels *via* PGE2 auto-secretion in rat VSMCs [28]. This is also consistent with previous studies of the mouse AC8 promoter that evidenced a cAMP response element (CRE) located 14 bp upstream of the putative transcription start site and required for basal and fsk-induced promoter activity [27,57]. This CRE is conserved in the rat and human AC8 promoters (FindM software, Eukaryotic Promoter Database). *In silico* analyses also brought out two highly conserved binding sites for AP-1 transcription factors and one E-box possibly interacting with HES7 and SNAI2 in the rat, mouse and human AC8 promoters. These motifs are located 3464 bp, 2244 bp and 1634 bp upstream of the rat translation start site, respectively. AP-1 dimers are transcriptional activators induced by inflammation while HES7 is a transcriptional repressor activated by the Notch signaling pathway. Consistently, we showed that AC8 induction in IL-1β-tdVSMCs partly depends on Notch signaling inhibition [8]. SNAI2 can act as a repressor or an activator of transcription and participates in epithelial–mesenchymal transition (EMT) [58]. Its implication in AC8E-H expression, although attractive since EMT and VSMC transdifferentiation may involve comparable mechanisms, remains to be explored.

The rat AC8 pre-mRNA is spliced into AC8E-H *via* an alternative 5' donor splice site (E5SS) that is conserved in humans (bp 547 to 555 in exon 1; Human Splicing Finder 3.1 software). The analysis of the exon 1 in both species revealed potential exonic splicing enhancer (ESE) motifs for serine/arginine-rich (SR) splicing factors in close proximity to the E5SS. In particular, we observed several putative binding sites for the serine/arginine-rich splicing factor 1 (SRSF1), which is known to participate in pressure-overload cardiac hypertrophy [59]. Whether SFRF1 and other splicing factors involved in the phenotypic modulation of VSMCs such as Quaking and ADAR1 [60,61] participate in AC8 pre-mRNA processing is currently under investigation.

Our discovery of novel AC splice variants specifically expressed in the pathological context of vascular remodeling is relevant to various diseases related to splicing defects, including cancers and neurological diseases [62]. The generation of AC alternative splice variants may therefore be part of a more general strategy of cell adaptation to its environment, the scope of which was previously unknown. Consistent with this, Katsushika and collaborators have described an AC5-alpha subvariant in dog heart encoding the first half of the enzyme only [63]. This variant is of particular interest because the heterodimerization motifs of the AC6 isoform, which

ACCEPTED MANUSCRIPT

belongs to the same family as AC5, appeared to be located in the M1 cassette [33]. There is growing evidence in favor of a functional impact of splice variants [64,65] but the causal contribution of disease-associated splice variants to the disease remains unclear in most cases. The functional assessment of AC5 and 8 splice variants in the heart and vessels could pave the way for further studies of the splice variants specifically expressed in a pathological context.

ACCEPTED MANUSCRIPT

ACCEPTED MANUSCRIPT

Acknowledgments

We would like to thank S. Bolte and JF. Gilles from the imaging facility of the Paris-Seine Biological Institute (IBPS), C. Dessauer for providing the AC3 construct, JB. Klarenbeek for providing the $^{T}Epac^{VV}$ expression plasmid, M. Babiak and E. Saylam for technical assistance in western blot and PCR experiments of the revised manuscript.

This work was supported by ANR grant 11BSV103401, the Lefoulon-Delalande Foundation, the French Federation of Cardiology (F.F.C), the *Nouvelle Société Francophone d'Athérosclérose* (NSFA), the *Société Française de Cardiologie* (SFC) and the *Groupe de Réflexion sur la Recherche Cardiovasculaire* (GRRC).

Author contributions

R.B and I.L came up with the initial concept for this study. B.V, Y.L-C, and R.B performed the key experiments. N.C constructed the $^{T}Epac^{VV}$-encoding adenovirus. M.G performed some of the PCR experiments. B.V, P.V, IL and R.B designed the study and the experiments and B.V, L.D, P.V, R.B and I.L interpreted the data. B.V, R.B, PV and I.L wrote the manuscript. Experiments were performed in the laboratories of P.V and I.L.

Conflict of interest

None declared.

ACCEPTED MANUSCRIPT

References

[1] N. Defer, M. Best-Belpomme, J. Hanoune, Tissue specificity and physiological relevance of various isoforms of adenylyl cyclase, Am. J. Physiol. Renal Physiol. 279 (2000) F400-416.

[2] R.K. Sunahara, C.W. Dessauer, A.G. Gilman, Complexity and diversity of mammalian adenylyl cyclases, Annu. Rev. Pharmacol. Toxicol. 36 (1996) 461–480. doi:10.1146/annurev.pa.36.040196.002333.

[3] A. Marjamaki, M. Sato, R. Bouet-Alard, Q. Yang, I. Limon-Boulez, C. Legrand, S.M. Lanier, Factors determining the specificity of signal transduction by guanine nucleotide-binding protein-coupled receptors. Integration of stimulatory and inhibitory input to the effector adenylyl cyclase, J. Biol. Chem. 272 (1997) 16466–16473.

[4] J.G. Webb, P.W. Yates, Q. Yang, Y.V. Mukhin, S.M. Lanier, Adenylyl cyclase isoforms and signal integration in models of vascular smooth muscle cells, Am. J. Physiol. Heart Circ. Physiol. 281 (2001) H1545-1552.

[5] R. Gros, Q. Ding, J. Chorazyczewski, J.G. Pickering, L.E. Limbird, R.D. Feldman, Adenylyl cyclase isoform-selective regulation of vascular smooth muscle proliferation and cytoskeletal reorganization, Circ. Res. 99 (2006) 845–852. doi:10.1161/01.RES.0000245189.21703.c0.

[6] U. Yokoyama, S. Minamisawa, A. Katayama, T. Tang, S. Suzuki, K. Iwatsubo, S. Iwasaki, R. Kurotani, S. Okumura, M. Sato, S. Yokota, H.K. Hammond, Y. Ishikawa, Differential regulation of vascular tone and remodeling via stimulation of type 2 and type 6 adenylyl cyclases in the ductus arteriosus, Circ. Res. 106 (2010) 1882–1892. doi:10.1161/CIRCRESAHA.109.214924.

[7] N. Clément, M. Glorian, M. Raymondjean, M. Andréani, I. Limon, PGE2 amplifies the effects of IL-1beta on vascular smooth muscle cell de-differentiation: a consequence of the versatility of PGE2 receptors 3 due to the emerging expression of adenylyl cyclase 8, J. Cell. Physiol. 208 (2006) 495–505. doi:10.1002/jcp.20673.

[8] Z. Keuylian, J.H.F. de Baaij, M. Gueguen, M. Glorian, C. Rouxel, E. Merlet, L. Lipskaia, R. Blaise, V. Mateo, I. Limon, The Notch pathway attenuates interleukin 1β (IL1β)-mediated induction of adenylyl cyclase 8 (AC8) expression during vascular smooth muscle cell (VSMC) trans-differentiation, J. Biol. Chem. 287 (2012) 24978–24989.

ACCEPTED MANUSCRIPT

doi:10.1074/jbc.M111.292516.

[9] R.S. Ostrom, X. Liu, B.P. Head, C. Gregorian, T.M. Seasholtz, P.A. Insel, Localization of adenylyl cyclase isoforms and G protein-coupled receptors in vascular smooth muscle cells: expression in caveolin-rich and noncaveolin domains, Mol. Pharmacol. 62 (2002) 983–992.

[10] M. Gueguen, Z. Keuylian, V. Mateo, N. Mougenot, A.-M. Lompré, J.-B. Michel, O. Meilhac, L. Lipskaia, I. Limon, Implication of adenylyl cyclase 8 in pathological smooth muscle cell migration occurring in rat and human vascular remodelling, J. Pathol. 221 (2010) 331–342. doi:10.1002/path.2716.

[11] M. Gueguen, B. Vallin, M. Glorian, R. Blaise, I. Limon, Adénylyl cyclases et transdifférenciation des cellules musculaires lisses vasculaires : rôle dans le remodelage vasculaire pathologique, Biol. Aujourdhui. 210 (2016) 153–166. doi:10.1051/jbio/2016020.

[12] J.S. McKean, F. Murray, G. Gibson, D.A. Shewan, S.J. Tucker, G.F. Nixon, The cAMP-producing agonist beraprost inhibits human vascular smooth muscle cell migration via exchange protein directly activated by cAMP, Cardiovasc. Res. 107 (2015) 546–555. doi:10.1093/cvr/cvv176.

[13] R.C. Hewer, G.B. Sala-Newby, Y.-J. Wu, A.C. Newby, M. Bond, PKA and Epac synergistically inhibit smooth muscle cell proliferation, J. Mol. Cell. Cardiol. 50 (2011) 87–98. doi:10.1016/j.yjmcc.2010.10.010.

[14] P.K. Vadiveloo, E.L. Filonzi, H.R. Stanton, J.A. Hamilton, G1 phase arrest of human smooth muscle cells by heparin, IL-4 and cAMP is linked to repression of cyclin D1 and cdk2, Atherosclerosis. 133 (1997) 61–69.

[15] N. Begum, S. Hockman, V.C. Manganiello, Phosphodiesterase 3A (PDE3A) deletion suppresses proliferation of cultured murine vascular smooth muscle cells (VSMCs) via inhibition of mitogen-activated protein kinase (MAPK) signaling and alterations in critical cell cycle regulatory proteins, J. Biol. Chem. 286 (2011) 26238–26249. doi:10.1074/jbc.M110.214155.

[16] S. Hayashi, R. Morishita, H. Matsushita, H. Nakagami, Y. Taniyama, T. Nakamura, M. Aoki, K. Yamamoto, J. Higaki, T. Ogihara, Cyclic AMP inhibited proliferation of human aortic vascular smooth muscle cells, accompanied by induction of p53 and p21, Hypertens. Dallas Tex 1979. 35 (2000) 237–243.

[17] D. Palmer, K. Tsoi, D.H. Maurice, Synergistic inhibition of vascular smooth muscle cell migration by phosphodiesterase 3 and phosphodiesterase 4 inhibitors, Circ. Res. 82 (1998) 852–

ACCEPTED MANUSCRIPT

861.

[18] S.J. Netherton, S.L. Jimmo, D. Palmer, D.G. Tilley, H.A. Dunkerley, D.R. Raymond, J.C. Russell, P.M. Absher, E.H. Sage, R.B. Vernon, D.H. Maurice, Altered phosphodiesterase 3-mediated cAMP hydrolysis contributes to a hypermotile phenotype in obese JCR:LA-cp rat aortic vascular smooth muscle cells: implications for diabetes-associated cardiovascular disease, Diabetes. 51 (2002) 1194–1200.

[19] A. Chatterjee, A. Sharma, M. Chen, R. Toy, G. Mottola, M.S. Conte, The pro-resolving lipid mediator maresin 1 (MaR1) attenuates inflammatory signaling pathways in vascular smooth muscle and endothelial cells, PloS One. 9 (2014) e113480. doi:10.1371/journal.pone.0113480.

[20] Y. Cai, D.J. Nagel, Q. Zhou, K.D. Cygnar, H. Zhao, F. Li, X. Pi, P.A. Knight, C. Yan, Role of cAMP-phosphodiesterase 1C signaling in regulating growth factor receptor stability, vascular smooth muscle cell growth, migration, and neointimal hyperplasia, Circ. Res. 116 (2015) 1120–1132. doi:10.1161/CIRCRESAHA.116.304408.

[21] C. Indolfi, E. Di Lorenzo, A. Rapacciuolo, A.M. Stingone, E. Stabile, A. Leccia, D. Torella, R. Caputo, F. Ciardiello, G. Tortora, M. Chiariello, 8-chloro-cAMP inhibits smooth muscle cell proliferation in vitro and neointima formation induced by balloon injury in vivo, J. Am. Coll. Cardiol. 36 (2000) 288–293.

[22] Y. Inoue, K. Toga, T. Sudo, K. Tachibana, S. Tochizawa, Y. Kimura, Y. Yoshida, H. Hidaka, Suppression of arterial intimal hyperplasia by cilostamide, a cyclic nucleotide phosphodiesterase 3 inhibitor, in a rat balloon double-injury model, Br. J. Pharmacol. 130 (2000) 231–241. doi:10.1038/sj.bjp.0703287.

[23] Y. Sassi, L. Lipskaia, G. Vandecasteele, V.O. Nikolaev, S.N. Hatem, F. Cohen Aubart, F.G. Russel, N. Mougenot, C. Vrignaud, P. Lechat, A.-M. Lompré, J.-S. Hulot, Multidrug resistance-associated protein 4 regulates cAMP-dependent signaling pathways and controls human and rat SMC proliferation, J. Clin. Invest. 118 (2008) 2747–2757. doi:10.1172/JCI35067.

[24] J.J. Cali, R.S. Parekh, J. Krupinski, Splice variants of type VIII adenylyl cyclase. Differences in glycosylation and regulation by Ca2+/calmodulin, J. Biol. Chem. 271 (1996) 1089–1095.

[25] N. Defer, O. Marinx, D. Stengel, A. Danisova, V. Iourgenko, I. Matsuoka, D. Caput, J. Hanoune, Molecular cloning of the human type VIII adenylyl cyclase, FEBS Lett. 351 (1994)

ACCEPTED MANUSCRIPT

109–113.

[26] D. Delmeire, D. Flamez, S.A. Hinke, J.J. Cali, D. Pipeleers, F. Schuit, Type VIII adenylyl cyclase in rat beta cells: coincidence signal detector/generator for glucose and GLP-1, Diabetologia. 46 (2003) 1383–1393. doi:10.1007/s00125-003-1203-8.

[27] L.M. Muglia, M.L. Schaefer, S.K. Vogt, G. Gurtner, A. Imamura, L.J. Muglia, The 5'-flanking region of the mouse adenylyl cyclase type VIII gene imparts tissue-specific expression in transgenic mice, J. Neurosci. Off. J. Soc. Neurosci. 19 (1999) 2051–2058.

[28] K. Blirando, R. Blaise, N. Gorodnaya, C. Rouxel, O. Meilhac, P. Vincent, I. Limon, The stellate vascular smooth muscle cell phenotype is induced by IL-1β via the secretion of PGE2 and subsequent cAMP-dependent protein kinase A activation, Biochim. Biophys. Acta. 1853 (2015) 3235–3247. doi:10.1016/j.bbamcr.2015.09.019.

[29] A.C. Conti, J.W. Maas, L.M. Muglia, B.A. Dave, S.K. Vogt, T.T. Tran, E.J. Rayhel, L.J. Muglia, Distinct regional and subcellular localization of adenylyl cyclases type 1 and 8 in mouse brain, Neuroscience. 146 (2007) 713–729. doi:10.1016/j.neuroscience.2007.01.045.

[30] M. Pagano, M.A. Clynes, N. Masada, A. Ciruela, L.-J. Ayling, S. Wachten, D.M.F. Cooper, Insights into the residence in lipid rafts of adenylyl cyclase AC8 and its regulation by capacitative calcium entry, Am. J. Physiol. Cell Physiol. 296 (2009) C607-619. doi:10.1152/ajpcell.00488.2008.

[31] J.B. Klarenbeek, J. Goedhart, M.A. Hink, T.W.J. Gadella, K. Jalink, A mTurquoise-based cAMP sensor for both FLIM and ratiometric read-out has improved dynamic range, PloS One. 6 (2011) e19170. doi:10.1371/journal.pone.0019170.

[32] A.C.L. Martin, D. Willoughby, A. Ciruela, L.-J. Ayling, M. Pagano, S. Wachten, A. Tengholm, D.M.F. Cooper, Capacitative Ca2+ entry via Orai1 and stromal interacting molecule 1 (STIM1) regulates adenylyl cyclase type 8, Mol. Pharmacol. 75 (2009) 830–842. doi:10.1124/mol.108.051748.

[33] Q. Ding, R. Gros, J. Chorazyczewski, S.S.G. Ferguson, R.D. Feldman, Isoform-specific regulation of adenylyl cyclase function by disruption of membrane trafficking, Mol. Pharmacol. 67 (2005) 564–571. doi:10.1124/mol.104.006817.

[34] C. Gu, J.J. Cali, D.M.F. Cooper, Dimerization of mammalian adenylate cyclases, Eur. J. Biochem. 269 (2002) 413–421.

[35] L.S. Shankman, D. Gomez, O.A. Cherepanova, M. Salmon, G.F. Alencar, R.M. Haskins, P. Swiatlowska, A.A.C. Newman, E.S. Greene, A.C. Straub, B. Isakson, G.J.

ACCEPTED MANUSCRIPT

Randolph, G.K. Owens, KLF4-dependent phenotypic modulation of smooth muscle cells has a key role in atherosclerotic plaque pathogenesis, Nat. Med. 21 (2015) 628–637. doi:10.1038/nm.3866.

[36] S.D. Rybalkin, K.E. Bornfeldt, W.K. Sonnenburg, I.G. Rybalkina, K.S. Kwak, K. Hanson, E.G. Krebs, J.A. Beavo, Calmodulin-stimulated cyclic nucleotide phosphodiesterase (PDE1C) is induced in human arterial smooth muscle cells of the synthetic, proliferative phenotype, J. Clin. Invest. 100 (1997) 2611–2621. doi:10.1172/JCI119805.

[37] S.D. Rybalkin, I. Rybalkina, J.A. Beavo, K.E. Bornfeldt, Cyclic nucleotide phosphodiesterase 1C promotes human arterial smooth muscle cell proliferation, Circ. Res. 90 (2002) 151–157.

[38] D.G. Tilley, D.H. Maurice, Vascular smooth muscle cell phenotype-dependent phosphodiesterase 4D short form expression: role of differential histone acetylation on cAMP-regulated function, Mol. Pharmacol. 68 (2005) 596–605. doi:10.1124/mol.105.014126.

[39] M.D. Houslay, The long and short of vascular smooth muscle phosphodiesterase-4 as a putative therapeutic target, Mol. Pharmacol. 68 (2005) 563–567. doi:10.1124/mol.105.015719.

[40] J.S. Douglas, D.R. Holmes, D.J. Kereiakes, C.L. Grines, E. Block, Z.M.B. Ghazzal, D.C. Morris, H. Liberman, K. Parker, C. Jurkovitz, N. Murrah, J. Foster, P. Hyde, G.B.J. Mancini, W.S. Weintraub, Cilostazol for Restenosis Trial (CREST) Investigators, Coronary stent restenosis in patients treated with cilostazol, Circulation. 112 (2005) 2826–2832. doi:10.1161/CIRCULATIONAHA.104.530097.

[41] N. Katakami, Y.-S. Kim, R. Kawamori, Y. Yamasaki, The phosphodiesterase inhibitor cilostazol induces regression of carotid atherosclerosis in subjects with type 2 diabetes mellitus: principal results of the Diabetic Atherosclerosis Prevention by Cilostazol (DAPC) study: a randomized trial, Circulation. 121 (2010) 2584–2591. doi:10.1161/CIRCULATIONAHA.109.892414.

[42] C. Gu, A. Sorkin, D.M. Cooper, Persistent interactions between the two transmembrane clusters dictate the targeting and functional assembly of adenylyl cyclase, Curr. Biol. CB. 11 (2001) 185–190.

[43] T. Seebacher, J.U. Linder, J.E. Schultz, An isoform-specific interaction of the membrane anchors affects mammalian adenylyl cyclase type V activity, Eur. J. Biochem. 268 (2001) 105–110.

[44] A. Baragli, M.-L. Grieco, P. Trieu, L.R. Villeneuve, T.E. Hébert, Heterodimers of

ACCEPTED MANUSCRIPT

adenylyl cyclases 2 and 5 show enhanced functional responses in the presence of Galpha s, Cell. Signal. 20 (2008) 480–492. doi:10.1016/j.cellsig.2007.10.033.

[45] A. Senes, M. Gerstein, D.M. Engelman, Statistical analysis of amino acid patterns in transmembrane helices: the GxxxG motif occurs frequently and in association with beta-branched residues at neighboring positions, J. Mol. Biol. 296 (2000) 921–936. doi:10.1006/jmbi.1999.3488.

[46] D. Willoughby, N. Masada, S. Wachten, M. Pagano, M.L. Halls, K.L. Everett, A. Ciruela, D.M.F. Cooper, AKAP79/150 interacts with AC8 and regulates Ca2+-dependent cAMP synthesis in pancreatic and neuronal systems, J. Biol. Chem. 285 (2010) 20328–20342. doi:10.1074/jbc.M110.120725.

[47] R.E. Simpson, A. Ciruela, D.M.F. Cooper, The role of calmodulin recruitment in Ca2+ stimulation of adenylyl cyclase type 8, J. Biol. Chem. 281 (2006) 17379–17389. doi:10.1074/jbc.M510992200.

[48] D. Willoughby, K.L. Everett, M.L. Halls, J. Pacheco, P. Skroblin, L. Vaca, E. Klussmann, D.M.F. Cooper, Direct binding between Orai1 and AC8 mediates dynamic interplay between Ca2+ and cAMP signaling, Sci. Signal. 5 (2012) ra29. doi:10.1126/scisignal.2002299.

[49] A.J. Crossthwaite, A. Ciruela, T.F. Rayner, D.M.F. Cooper, A direct interaction between the N terminus of adenylyl cyclase AC8 and the catalytic subunit of protein phosphatase 2A, Mol. Pharmacol. 69 (2006) 608–617. doi:10.1124/mol.105.018275.

[50] L.J. Ayling, S.J. Briddon, M.L. Halls, G.R.V. Hammond, L. Vaca, J. Pacheco, S.J. Hill, D.M.F. Cooper, Adenylyl cyclase AC8 directly controls its micro-environment by recruiting the actin cytoskeleton in a cholesterol-rich milieu, J. Cell Sci. 125 (2012) 869–886. doi:10.1242/jcs.091090.

[51] G. Zhang, Y. Liu, A.E. Ruoho, J.H. Hurley, Structure of the adenylyl cyclase catalytic core, Nature. 386 (1997) 247–253. doi:10.1038/386247a0.

[52] Y.L. Guo, T. Seebacher, U. Kurz, J.U. Linder, J.E. Schultz, Adenylyl cyclase Rv1625c of Mycobacterium tuberculosis: a progenitor of mammalian adenylyl cyclases, EMBO J. 20 (2001) 3667–3675. doi:10.1093/emboj/20.14.3667.

[53] M. Tanowitz, J.N. Hislop, M. von Zastrow, Alternative splicing determines the post-endocytic sorting fate of G-protein-coupled receptors, J. Biol. Chem. 283 (2008) 35614–35621. doi:10.1074/jbc.M806588200.

ACCEPTED MANUSCRIPT

[54] E. Hartmann, T.A. Rapoport, H.F. Lodish, Predicting the orientation of eukaryotic membrane-spanning proteins, Proc. Natl. Acad. Sci. U. S. A. 86 (1989) 5786–5790.

[55] M. Sato, R. Hresko, M. Mueckler, Testing the charge difference hypothesis for the assembly of a eucaryotic multispanning membrane protein, J. Biol. Chem. 273 (1998) 25203–25208.

[56] M. Bogdanov, W. Dowhan, H. Vitrac, Lipids and topological rules governing membrane protein assembly, Biochim. Biophys. Acta. 1843 (2014) 1475–1488. doi:10.1016/j.bbamcr.2013.12.007.

[57] J.R. Chao, Y.G. Ni, C.A. Bolaños, Z. Rahman, R.J. DiLeone, E.J. Nestler, Characterization of the mouse adenylyl cyclase type VIII gene promoter: regulation by cAMP and CREB, Eur. J. Neurosci. 16 (2002) 1284–1294.

[58] M.A. Nieto, The snail superfamily of zinc-finger transcription factors, Nat. Rev. Mol. Cell Biol. 3 (2002) 155–166. doi:10.1038/nrm757.

[59] T. Kim, J.O. Kim, J.G. Oh, S.-E. Hong, D.H. Kim, Pressure-overload cardiac hypertrophy is associated with distinct alternative splicing due to altered expression of splicing factors, Mol. Cells. 37 (2014) 81–87. doi:10.14348/molcells.2014.2337.

[60] E.P. van der Veer, R.G. de Bruin, A.O. Kraaijeveld, M.R. de Vries, I. Bot, T. Pera, F.M. Segers, S. Trompet, J.M. van Gils, M.K. Roeten, C.M. Beckers, P.J. van Santbrink, A. Janssen, C. van Solingen, J. Swildens, H.C. de Boer, E.A. Peters, R. Bijkerk, M. Rousch, M. Doop, J. Kuiper, M.J. Schalij, A.C. van der Wal, S. Richard, T.J.C. van Berkel, J.G. Pickering, P.S. Hiemstra, M.J. Goumans, T.J. Rabelink, A.A.F. de Vries, P.H.A. Quax, J.W. Jukema, E.A.L. Biessen, A.J. van Zonneveld, Quaking, an RNA-binding protein, is a critical regulator of vascular smooth muscle cell phenotype, Circ. Res. 113 (2013) 1065–1075. doi:10.1161/CIRCRESAHA.113.301302.

[61] J. Fei, X.-B. Cui, J.-N. Wang, K. Dong, S.-Y. Chen, ADAR1-Mediated RNA Editing, A Novel Mechanism Controlling Phenotypic Modulation of Vascular Smooth Muscle Cells, Circ. Res. 119 (2016) 463–469. doi:10.1161/CIRCRESAHA.116.309003.

[62] B. Chabot, L. Shkreta, Defective control of pre-messenger RNA splicing in human disease, J. Cell Biol. 212 (2016) 13–27. doi:10.1083/jcb.201510032.

[63] S. Katsushika, J. Kawabe, C.J. Homcy, Y. Ishikawa, In vivo generation of an adenylylcyclase isoform with a half-molecule motif, J. Biol. Chem. 268 (1993) 2273–2276.

[64] O. Kelemen, P. Convertini, Z. Zhang, Y. Wen, M. Shen, M. Falaleeva, S. Stamm,

ACCEPTED MANUSCRIPT

Function of alternative splicing, Gene. 514 (2013) 1–30. doi:10.1016/j.gene.2012.07.083.

[65] V. Pagliarini, C. Naro, C. Sette, Splicing Regulation: A Molecular Device to Enhance Cancer Cell Adaptation, BioMed Res. Int. 2015 (2015) 543067. doi:10.1155/2015/543067.

ACCEPTED MANUSCRIPT

ACCEPTED MANUSCRIPT

Highlights

- IL-1β-transdifferentiated VSMCs express short adenylyl cyclase isoforms termed AC8E-H
- AC8E-H result from alternative splicing and lack the first five transmembrane domains
- AC8E-H act as dominant-negatives by forming dimers with full-length adenylyl cyclases

ACCEPTED MANUSCRIPT